# TRUST

# High resolution monitoring, real time visualization and reliable modeling of highly controlled, intermediate and up-scalable size pilot injection tests of underground storage of $CO_2$

**Contract #309067**

| | |
|---|---|
| **Deliverable Number** | **D4.1** |
| **Title** | **Design simulations for the Heletz injection experiments** |
| **Work-Package** | **4** |

| | |
|---|---|
| **Lead Participant** | **UU** |
| **Contributors** | EWRE |

| | |
|---|---|
| **Version:** | **1** |
| **Revision level:** | **01** |
| **Date:** | **Month 36** |
| **Reviewed by:** | |
| **Status:** | **FINAL** |
| **Dissemination level** | **PU** |

# Design simulations for the Heletz Injection experiments

**Kristina Rasmusson[1], Saba Joodaki[1], Jacob Bensabat[2] and Auli Niemi[1]**

(1) Uppsala University, Department of Earth Sciences
(2) EWRE Ltd.

# Executive summary

This deliverable presents the findings of the investigations aimed at evaluating the effect of different modes of injection to enhance trapping, with the objective to provide design guidance to Heletz $CO_2$ injection experiments in TRUST project. Effect of varying various design parameters was evaluated as were a number of different injection strategies. Effect of geological heterogeneity was considered as well, this using a vertical models with radial symmetry and three dimensional models. The residual and dissolution trapping were determined and the results were compared using various trapping indicators. In all simulations total amounts and injection rates were selected according to the specifications of the Heletz site, i.e. a small-scale pilot test. We observed that the accuracy of the trapping model used for describing residual trapping is of major importance for the predicted residual trapping. The impact of the total amount of injected $CO_2$ and the $CO_2$ injection rate were evaluated. For the considered quantities of $CO_2$, the amount of the $CO_2$ has a large impact on the trapping. The residual trapping starts after the injection has ended, which allows the smaller amounts of injected $CO_2$ more time to redistribute and become trapped compared to when larger amounts of $CO_2$ is injected. Higher injection rates produced consistently more residual as well as overall trapping. For a given amount of $CO_2$, a higher injection rate corresponds to shorter injection duration and thereby a longer redistribution time in-situ and consequently more residual trapping. With regard to alternative modes of injection we conclude that more $CO_2$ trapping can be achieved if the CO2 injection is combined with water injection. A larger mass percent of water does not only increase the residual and solubility trapping but also the pressure increase in-situ. When using chase water injection after $CO_2$ injection, the solubility trapping was increased by a few percent. The residual trapping was also enhanced greatly during the chase water injection, but with time the difference decreased being less than 10 percent at the end of the observation period. All injection strategies except cyclic injection induce enhanced trapping when compared with conventional injection, mainly through increased residual trapping. Cyclic injection, as well as WAG injection strategies, can increase residual trapping greatly over a short time periods. The highest pressure increase was seen for strategies which combined injection of water and $CO_2$. When employing strategies consisting of chase water injections, residually trapped $CO_2$ is lacking in the vicinity of the well due to dissolution into the liquid phase. When using the 2-D model it could be seen that short after the injection ends the trapping in the heterogeneous case is higher than for the homogeneous case. At later times, however, the trapping becomes higher for the homogeneous case in comparison to most of the heterogeneous realizations. This is due to the fact that on longer time scales, heterogeneity is retarding the buoyant migration which results in less imbibition and thereby less residually trapped $CO_2$. The role of the two-dimensionality model in this result deserves further analysis.

A set of 3D simulations were also carried out, in order to evaluate the effect of selected injection strategies as well as geological heterogeneity on trapping. While being fully three-dimensional and thereby more representative of the true geology, the model also had some limitations in comparison to the previous 2D model, such as not including hysteresis. The model was therefore mainly at this stage used to look at dissolution trapping. Based on the 3D simulations following conclusions could be made: different injection patterns can be used to improve $CO_2$ dissolution trapping in saline aquifers. Injecting water after $CO_2$ injection, higher injection rate and having a pause in an injection cycle can be used to increase the $CO_2$ dissolution in the brine formation. It was also observed that dissolution index was higher in heterogeneous formations in comparison to homogeneous one.

The above simulations provide a good basis to decide which injection strategy to use at Heletz to achieve enhanced trapping. The final decision will be made once the first field results from the first set of simulations with 'conventional strategies' are available and can be used to calibrate the simulation models.

| Keywords | CO2 injection, solubility trapping, capillary trapping, heterogeneity, simulations. |
|---|---|

# Content

# 1. Nomenclature

| | | |
|---|---|---|
| $k_{rg}$ | Relative permeability to the gas phase | |
| $k_{rl}$ | Relative permeability to the liquid phase | |
| S | Saturation | |
| $S_{gr}^{\Delta}$ | Residual gas saturation | |
| $S_l^{\Delta}$ | Turning-point saturation | |
| $S_{grmax}$ | Maximum residual gas saturation | |
| $S_{lr}$ | Residual liquid-phase saturation | |
| $\bar{S}_l$ | Effective residual liquid saturation | $= \frac{S_l - S_{lr}}{1 - S_{lr}}$ |
| $\bar{S}_l^{\Delta}$ | Effective turning-point saturation | $= \frac{S_l^{\Delta} - S_{lr}}{1 - S_{lr}}$ |
| $\bar{S}_{gt}$ | Effective trapped gas-phase saturation | $= \frac{S_{gr}^{\Delta}(S_l - S_l^{\Delta})}{(1 - S_{lr})(1 - S_l^{\Delta} - S_{gr}^{\Delta})}$ |

# 2. Introduction and objectives

Within the TRUST project a series of $CO_2$ injection experiments will be carried out at the Heletz $CO_2$ injection site, with special focus on at how to enhance $CO_2$ trapping by different modes of injection

Two 'base case' $CO_2$ injection experiment sequences have been designed during the preceding MUSTANG project and are described in e.g. Rasmusson et al. (2014, 2015) and Fagerlund at al. (2013 a, b), as well as in several MUSTANG deliverables, especially the main summary reports and deliverables of Work Package 6 (www.co2mustang.eu): a single-well push-pull test for determining the in-situ residual trapping and a two-well dipole test for determining dissolution trapping. Extensive work has also been carried out to estimate how these different types of trapping can be determined in-situ by various indirect methods, in particular hydraulic, thermal and tracer testing methods (see the above articles). These base experiments (Experiment Set 1) are to be initiated shortly after the date of this report and will form a basis to the continuation experiments (Experiment Set 2) to be carried out within TRUST project, with the objective to see how trapping can be enhanced by various modes of injection.

The design simulations of these further experiments, with the specific objective to see how trapping can be enhanced by different modes of injection are described in this report. It should be pointed out that the actual test results of the Experiment Set 1, once available, will further guide the final design of Experiment Set 2.

# 3. Site Description

The test site is located at Heletz, Israel. It is part of a depleted oil field with a number of abandoned wells (Figure 1). The target layer is a non-continuous nearly 10m thick sandstone (shown as K, W and A sand layers in Figure 1) located at the depth of about 1600m. The layer is covered with a 40 m caprock layer. Two wells, an injection well and an abstraction well have been drilled and instrumented on the site for the purpose of $CO_2$ injection experiments during the preceding EU project MUSTANG (www.co2mustang.eu). Extensive characterization of the site has been carried out as described in Deliverables of the MUSTANG project (deliverables of Work Package 2 and 6, www.co2mustang.eu) and summarized in a journal article Niemi et al., (2016, to appear) and other articles of the same special edition (MUSTANG/Heletz Special Edition to International Journal of Greenhouse Gas Control, 2016).

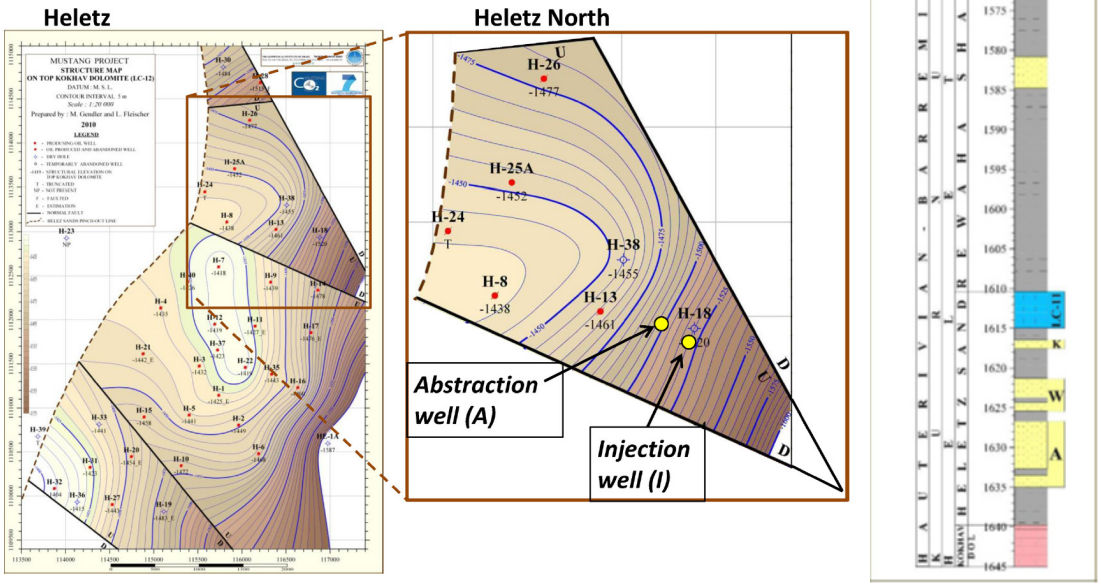
Heletz
Heletz North
MUSTANG PROJECT
STRUCTURE MAP
ON TOP KOKHAV DOLOMITE (LC-12)
H-26
-1477
H-25A
-1452
H-24
H-38
-1455
H-8
-1438
H-13
-1461
H-18
Abstraction well (A)
Injection well (I)
HELETZ - 18B
LITHOSTRATIGRAPHIC SECTION
DEPTH m
LITHOLOGY
LC-11
K
W
A

Figure 1a. Map of the target formation for $CO_2$ field injection experiments at Heletz, Israel, (based on the structure map by Gendler and Fleischer, in Erlström et al. (2010)) (left panel) and deep well profile showing the target layers (right panel)

Figure1b. Example instrumentation for $CO_2$ injection and sampling on the site

# 4. Numerical modeling of residual and solubility trapping

## 4.1 TOUGH2 simulations

The TOUGH2/iTOUGH2 simulator (Finsterle, 2007; Pruess et al., 1999) with the ECO2N module (Pruess, 2005) was used in this study. The simulator models two-phase flow of a $CO_2$-rich and water-rich phase. The components; $H_2O$, NaCl and $CO_2$ (and energy) are considered. Density, viscosity, specific enthalpy are treated as functions of the thermodynamic variables temperature, pressure, salinity and in some cases composition. Phase changes are identified and the phase compositions determined by the simulator. The solubility of both $CO_2$ and water in the phases is determined by a modified version of the partitioning model by Spycher and Pruess (2005) were Altunin's correlation is used to calculate the $CO_2$ molar volumes. Precipitation and dissolution of

NaCl are accounted for. The simulations were non-isothermal. The version of hysteretic capillary pressure and relative permeability functions implemented by Doughty (Doughty, 2008) into TOUGH2 was employed. These are a van Genuchten (1980) capillary pressure function, and a relative permeability function based on the work of Parker and Lenhard (1987), Lenhard and Parker (1987) and van Genuchten (1980), eq. 1-3. The capillary pressure function can describe; primary drainage, first-order scanning imbibition, second-order scanning drainage and third-order scanning imbibition. The relative permeability function has one branch for primary drainage and one for all other processes.

$$P_c = -P_0^{d,w}\left[\left(\frac{S_l - S_{l\,min}}{1 - S_{gr}^{\Delta} - S_{l\,min}}\right)^{-\left(\frac{1}{m^{d,w}}\right)} - 1\right]^{\left(1-m^{d,w}\right)} \quad \text{for } S_{l\,min} \le S_l \le 1 - S_{gr}^{\Delta} \tag{1}$$

$$k_{rl} = \sqrt{\bar{S}_l}\left[1 - \left(1 - \frac{\bar{S}_{gt}}{1-\bar{S}_l^{\Delta}}\right)\left(1 - \left(\bar{S}_l + \bar{S}_{gt}\right)^{1/m}\right)^{m} - \left(\frac{\bar{S}_{gt}}{1-\bar{S}_l^{\Delta}}\right)\left(1 - \left(\bar{S}_l^{\Delta}\right)^{1/m}\right)^{m}\right]^2 \quad \text{for } S_l \ge S_{lr} \tag{2}$$

$$k_{rg} = k_{rg\,max}\left(1 - \left(\bar{S}_l + \bar{S}_{gt}\right)\right)^{\gamma}\left(1 - \left(\bar{S}_l + \bar{S}_{gt}\right)^{1/m}\right)^{2m} \quad \text{for } S_l \ge S_{lr} \tag{3}$$

$\bar{S}_{gt}$ Is equal to zero during primary drainage.

As standard the code uses a modified Land's trapping model (1968), eq. 4, to determine the residual gas saturation.

$$S_{gr}^{\Delta} = \frac{1}{1/(1 - S_l^{\Delta}) + 1/S_{grmax} - 1/(1 - S_{lr})} \tag{4}$$

Parameter values for the capillary pressure and relative permeability functions were obtained by manually fitting the functions to Heletz-specific data (Benson et al., 2014). As these core samples had a *k* equal to 104 mD, Leverett scaling of the capillary pressure function ($P_0^d$ and $P_0^w$) was employed to convert to a k of 390 mD (mean for the core samples from the site and the *k* used as intrinsic permeability in the simulations).

The conceptual models used in the study are:

- A 2D slice with dip;
- 2D radially symmetric model (two different discretizations referred to as DISC 1 and DISC 2).

The "2D slice" conceptual model had three layers; sandstone, shale and sandstone again. The thicknesses of the layers in both wells were honored and the layers were therefore given increasing or decreasing thickness over the distance between the wells. The dip of the layers was also taken into consideration. The model was 40 meters long, corresponding to the distance between the injection and observation well at the Heletz field $CO_2$-injection-test site. The left and right boundary grid blocks represented the wells. No-flow boundary conditions were given to the bottom and top of the model. A grid block discretization of 0.25 m was used, except for the grid blocks representing the wells, which were smaller.

Two versions of 2D radially symmetric models with slightly different discretizations were used. They had three layers; sandstone, shale and sandstone again. Two, three and nine meters thick, respectively. Each model had a radius of 500 m.

- **DISC 1:** In the horizontal direction, one 0.09 m, 100 elements of 0.5 m and outside these 50 grid elements with logarithmically increasing radius out to a distance of 500 m from the well and finally a grid element with a volume such that the estimated layer volume was

fulfilled. In the vertical direction the model had a discretization of 0.5 m (total of 14 m). No-flow boundary conditions were given to the bottom and top of the model.

- **DISC 2:** In the horizontal direction, two 0.09 m, 100 elements with logarithmically increasing radius out to a distance of 500 m from the well and finally a grid element with a volume such that the estimated layer volume was fulfilled. In the vertical direction the model had a discretization of 0.25 m for sandstone layers and 0.5 for the shale layer (total of 14 m). No-flow boundary conditions were given to the bottom and top of the model.

The initial condition is a gravity equilibrium pressure gradient with depth.

In some parts of this study the geological heterogeneity of the sandstone layers is modeled. The related input parameters are derived from porosity data, based on resistivity well log data from three sandstone layers in the H18, H13 and H38 wells and a site-specific empirical poro-perm relationship, Olofsson (2011) found the variation in permeability in the vertical direction to be described well by a log-semivariogram with exponential model nugget factor=0, sill=0.526 and a=0.9, i.e. a correlation length of 2.7 m. However the horizontal correlation length is unknown and therefore has to be assumed. An angel of 90º for the variogram was specified and an anisotropy of 3.0 was used to make the horizontal correlation length 3 times larger than that in the vertical direction. In the simulations half the sill values was used as such a large variation in property values was not seen among the core samples.

Heterogeneous realizations of the permeability field were created with the Sequential Gaussian Simulation method within the iTOUGH2-GSLIB simulator (Finsterle, 2007; Finsterle and Kowalsky, 2007). The heterogeneous 2D radially symmetric models were somewhat simplified, as the heterogeneity was only applied to the two sandstone layers and restricted to a distance of 50 m from the well, outside this area the sandstone layers where assumed homogeneous. No two-phase flow was however observed outside this distance.

Other input parameters used in the simulations are given in Table 1.

Table 1. Input parameters for the simulations.

| Parameter | Value |
|---|---|
| *Sandstone* | |
| Grain density [g/cc] | 2645 |
| Porosity [-] | 0.2216 |
| Absolute permeability [mD or $m^2$] | 390 or 39.0e-14[a] |
| Pore compressibility [$Pa^{-1}$] | 4.5e-10 |
| | |
| *Shale* | |
| Grain density [g/cc] | 2555 |
| Porosity [-] | 0.06 |
| Absolute permeability [mD or $m^2$] | impermeable |

| | |
|---|---|
| Pore compressibility [$Pa^{-1}$] | 4.5e-10 |
| *Initial conditions* | |
| Temperature [ºC] | 60 |
| Salinity [salt mass fraction] | 0.05 |
| Pressure [Pa] at the bottom of the formation | 1.47e7 |
| Gravitational acceleration vector [$m/s^2$] | 9.81 |

[a]Mean *k* for core samples.

## 4.2 **Code developments made for the study**

Some non-standard features were added to the TOUGH2 code, in order to carry out the simulations. These included:

- The porosity can be selected to be correlated with the absolute permeability of each grid block (following a Heletz-site specific relationship).
- Leverett-scaling of the capillary pressure with regard to both porosity and permeability ($P_c = P_c^{ref} \cdot \sqrt{k^{ref} \cdot \varphi / k \cdot \varphi^{ref}}$). This scaling can be selected as an option to the standard one, i.e. scaling with regard to permeability only.
- Additional trapping model options ($S_{gi}$-$S_{gr}$ relationships). Aissaoui's law and the Jerauld trapping model were added.

The original hysteretic TOUGH2 code contains a modified version of Land's trapping model. To study the effect of assumptions regarding the $S_{gr}$-$S_{gi}$ relationship on the amount of $CO_2$ trapped by different trapping mechanisms (residual and dissolution), additional trapping models were added. The added trapping models include the Aissaoui's (1983, through Suzanne et al. (2003)), eq. 5-6 and Jerauld's (1997), eq. 7, trapping models. $S_{go}$ should be in the range 0.6 to 0.7 if the porosity is larger than 0.13, here the value 0.6 was used. These are also shown in Figure 4.1.

$$S_{gr} = \frac{S_{grm}}{S_{go}} \cdot S_{gi}, \qquad for\ S_{gi} < S_{go} \tag{5}$$

$$S_{gr} = S_{grm}, \qquad for\ S_{gi} \geq S_{go} \tag{6}$$

$$S_{gr} = \frac{S_{gi}}{1 + \left(\frac{1}{S_{grm}} - 1\right) \cdot S_{gi}^{\left(\frac{1}{1 - S_{grm}}\right)}} \tag{7}$$

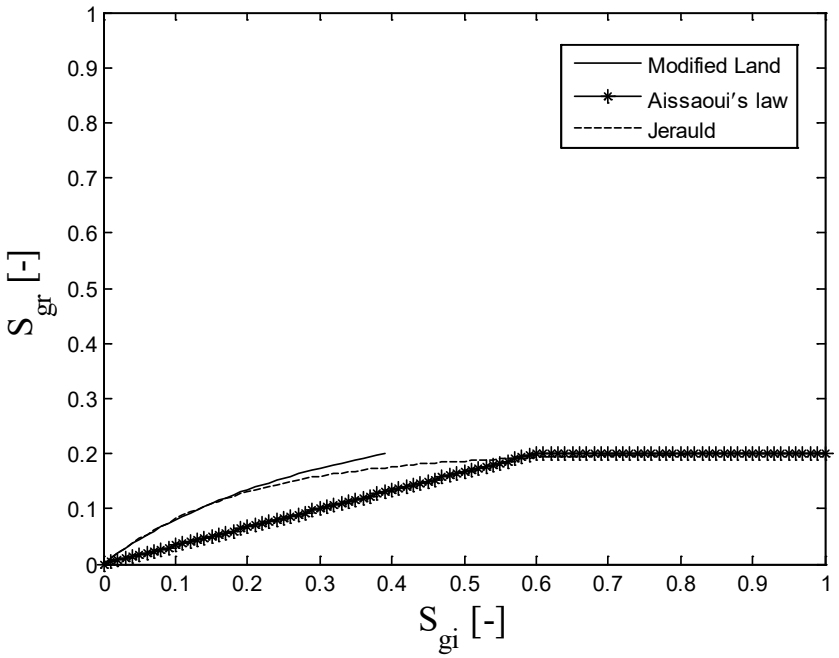


**Figure 4.1:** Trapping models when assuming $S_{grm}$=0.2.

# 5. Simulated scenarios (2D and 2D radially symmetrical models)

The numerical study included:

- Using different trapping models ($S_{gi}$-$S_{gr}$ relationships) to evaluate their importance.
- Evaluation of different injection strategies to enhance dissolution or residual trapping, see Table 2.
- A comparison of results from injection into a homogenous formation to results from injection into geologically heterogeneous sandstone layers (multiple permeability/porosity-fields).

Table 2. Alternative injection strategies.

| Injection strategy | |
|---|---|
| Strategy 1 ('Conventional injection') | -$CO_2$ injection (500 tons, 1 kg/s) |
| Strategy 2 ( 'Chased injection) | -$CO_2$ injection (500 tons, 1 kg/s)<br>-Chase water injection (125 tons, 0.8 kg/s) |
| Strategy 3 ('Co-injection') | -Co-injection of $CO_2$ with a small portion of water (500 tons, 1 kg/s and 85 tons, 0.17 kg/s, respectively)[A] |
| Strategy 4 ( 'Mixed co-injection and chased injection') | -Co-injection of $CO_2$ with a small portion of water (500 tons, 1 kg/s and 85 tons, 0.17 kg/s, respectively)<br>-Chase water injection (125 tons, 0.8 kg/s) |
| Strategy 5 ( 'Cyclic injection') | -$CO_2$ injection (250 tons, 1 kg/s)<br>-Break (0.9 days)<br>-$CO_2$ injection (250 tons, 1 kg/s) |
| Strategy 6 ( 'Small WAG injection') | -$CO_2$ injection (250 tons, 1 kg/s)<br>-Water injection (62.5 tons, 0.8 kg/s)<br>-$CO_2$ injection (250 tons, 1 kg/s)<br>-Water injection (62.5 tons, 0.8 kg/s) |

[C]Corresponds to 0.10 volumetric flow of water during co-injection.

The 'conventional injection' strategy means that the $CO_2$ is injected and then left to redistribute in the formation without any interference. The 'chased injection' strategy consists of a $CO_2$ injection followed by a water injection. The 'co-injection' strategy means that a small amount of water is injected simultaneous as the $CO_2$ is injected. The 'mixed co-injection and chased injection' strategy combines both of the two previous strategies. In the 'cyclic injection' strategy the $CO_2$ injection is partitioned into two smaller injections (each containing half of the total $CO_2$ to be injected) and a small break is made in between the injections, allowing the $CO_2$ to redistribute. The 'small WAG injection' strategy consists of two WAG cycles. One cycle is a $CO_2$ injection and a following chase water injection. The WAG strategy is therefore similar to the cyclic injection but with chase water stages instead of breaks, in between the $CO_2$ injections.

# 6. Results from the numerical modeling of residual and solubility trapping

To quantify the trapping, the trapping indexes (RTI, STI and TEI) used by Nghiem et al. (2009) were employed. The residual gas trapping index, RTI(t), is the ratio of total residual $CO_2$ mass

at time t, to the total mass of $CO_2$ injected at time t. The solubility trapping index, STI(t), is the total mass of $CO_2$ dissolved in the brine at time t, to the total mass of $CO_2$ injected at time t. The trapping efficiency index, TEI(t), is the sum of RTI(t) and STI(t).

## 6.1 **Impact of trapping model on trapping**

The effect of using different assumptions regarding the $S_{gi}$-$S_{gr}$ relationship (i.e. trapping models) was studied. The simulated scenario was 1 day of $CO_2$ injection followed by buoyant migration in a dipping formation with two high permeable layers (2D slice with dip). The total observation time was 10 days from the start of injection. The geometry and conditions of the layers followed those at the Heletz test site between the injection and observation well. Simulation results are shown in Figure 6.1 to Figure 6.9.

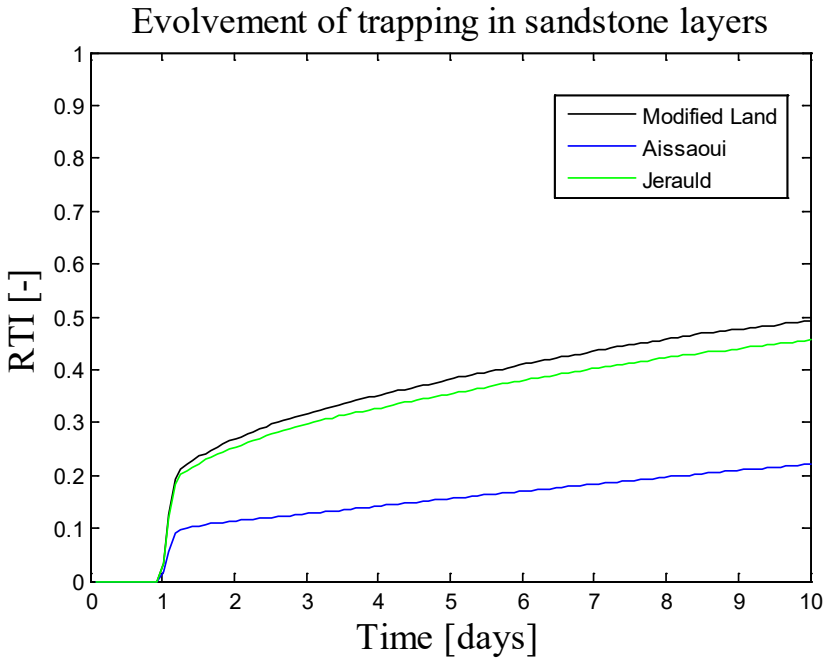


**Figure 6.1:** Residual trapping index (RTI) when using different trapping models.

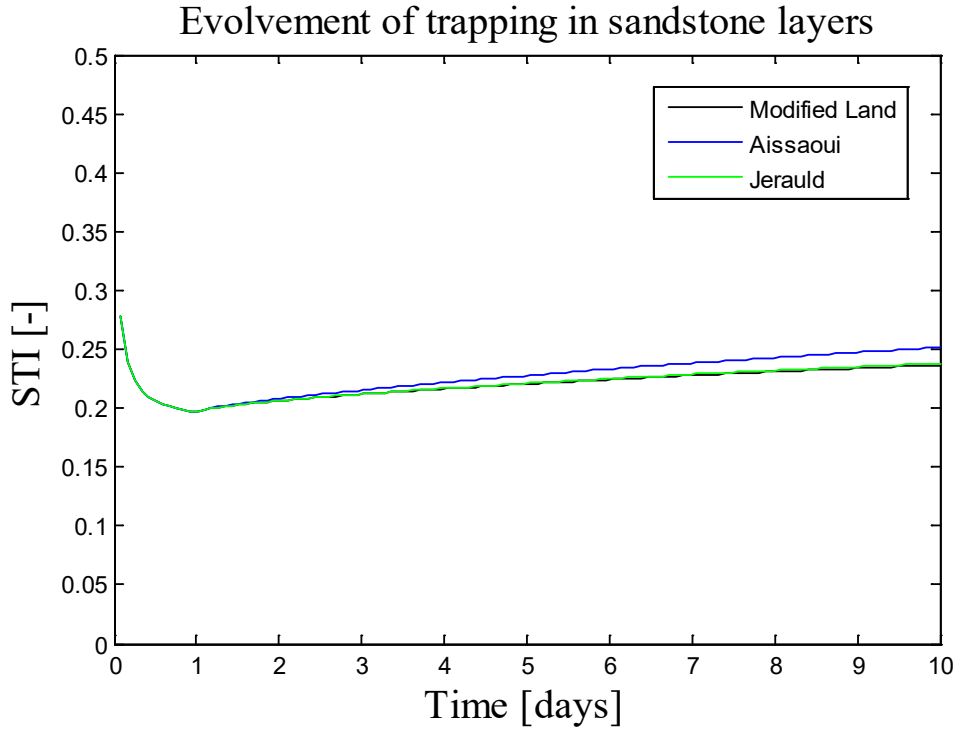


**Figure 6.2:** Solubility trapping index (STI) when using different trapping models.

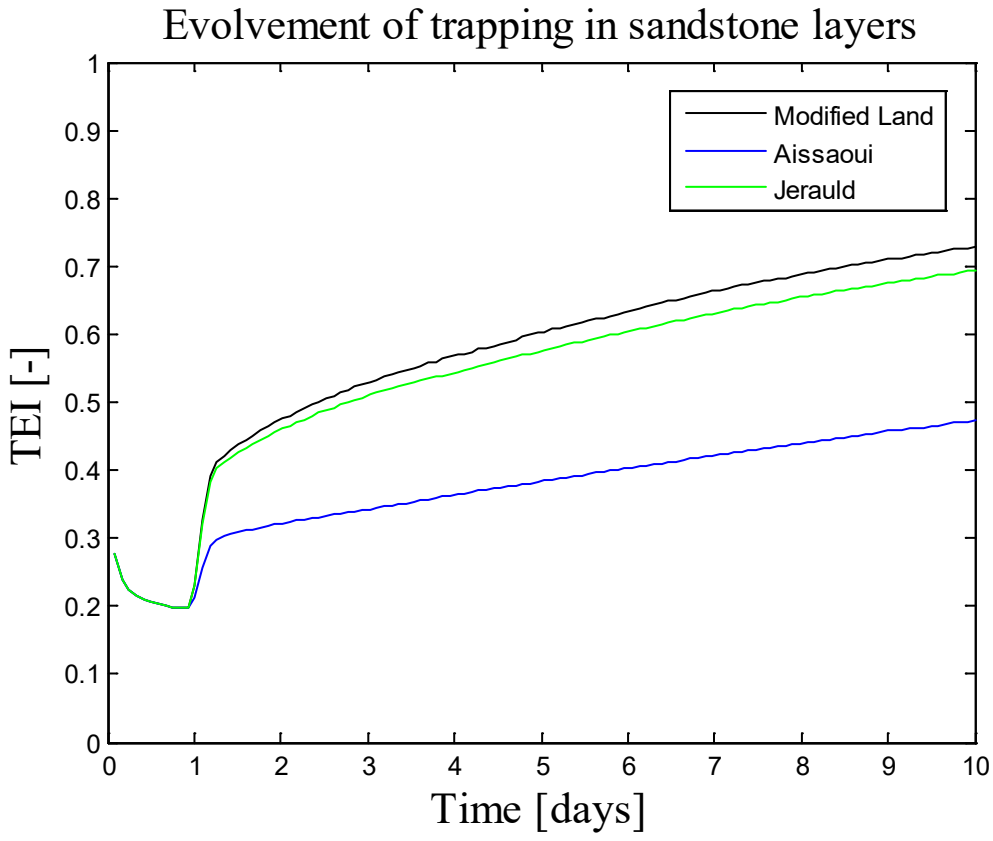


**Figure 6.3:** Trapping efficiency index (TEI) when using different trapping models.

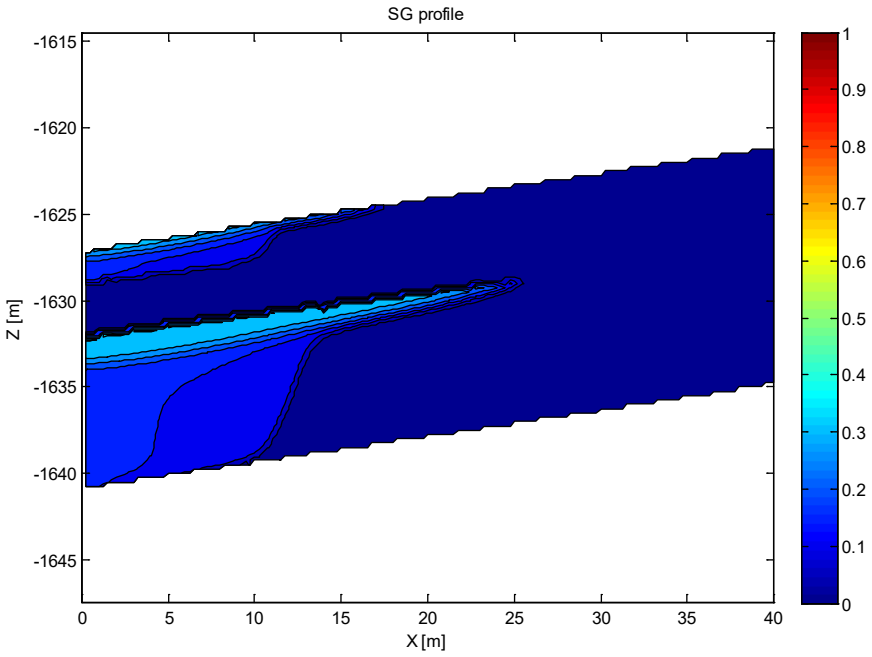


**Figure 6.4:** "Gas" saturation at time=10 days when using the (standard) modified Land trapping model.

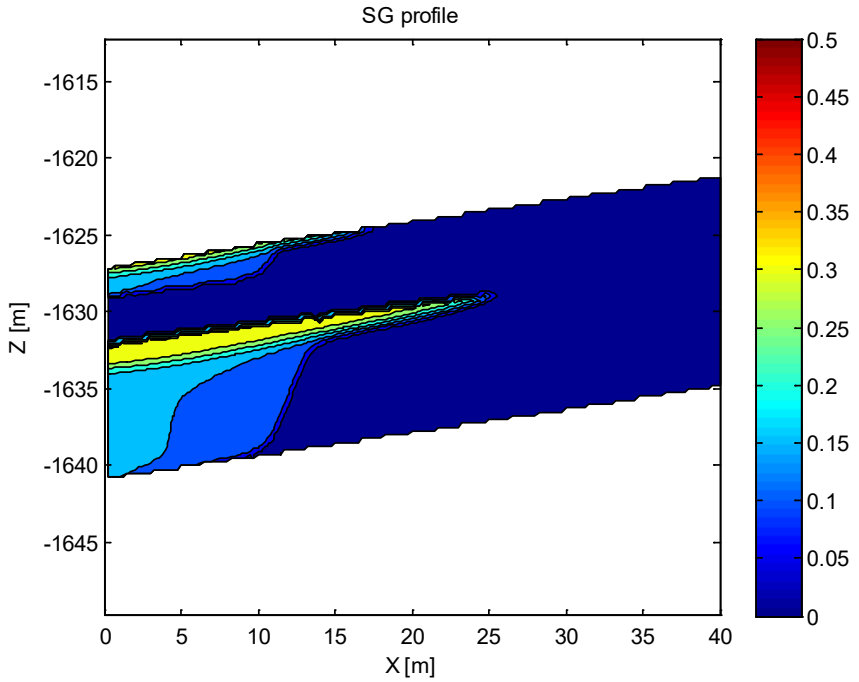


**Figure 6.5:** "Gas" saturation at time=10 with a different color map scale than in Figure 6.4 when using the modified Land trapping model (standard).

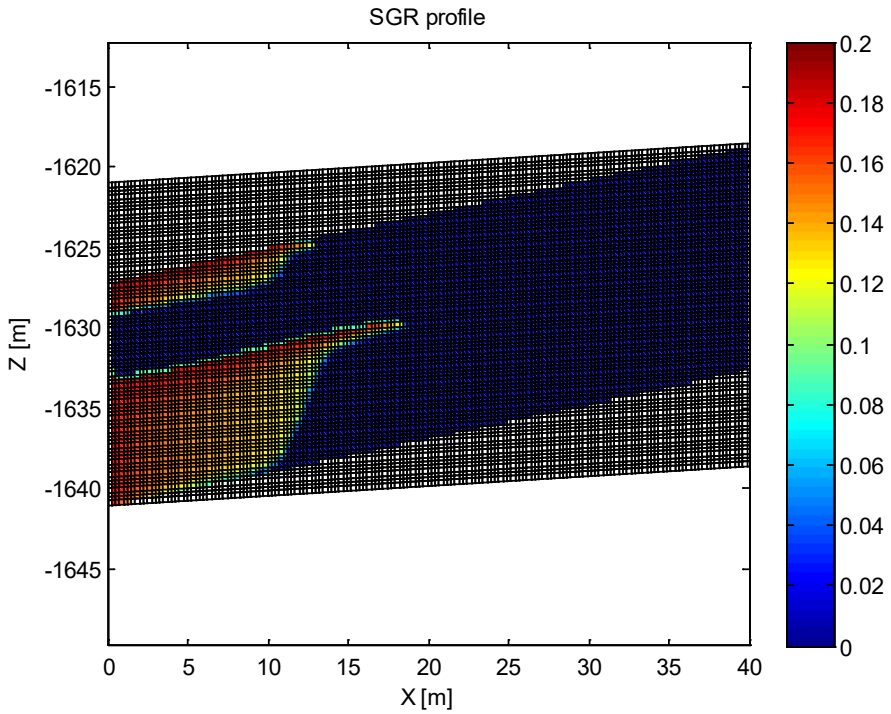


**Figure 6.6:** Residual "gas" saturation at time=10 days using the modified Land trapping model (standard).

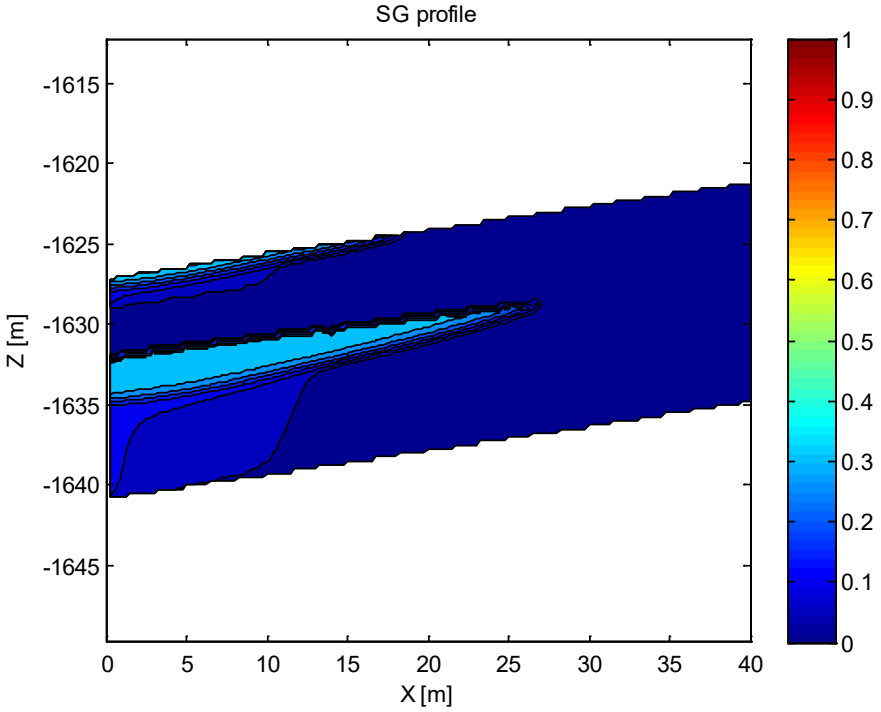


**Figure 6.7:** "Gas" saturation at time=10 days using the Aissaoui trapping model.

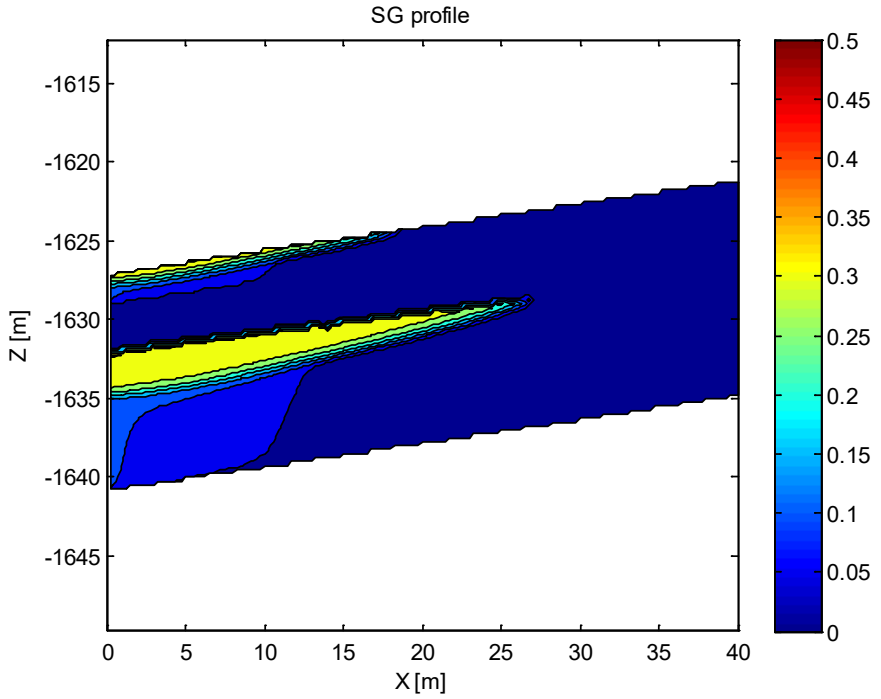


**Figure 6.8:** Same as figure the above, but with a different color map scale when using the Aissaoui trapping model.

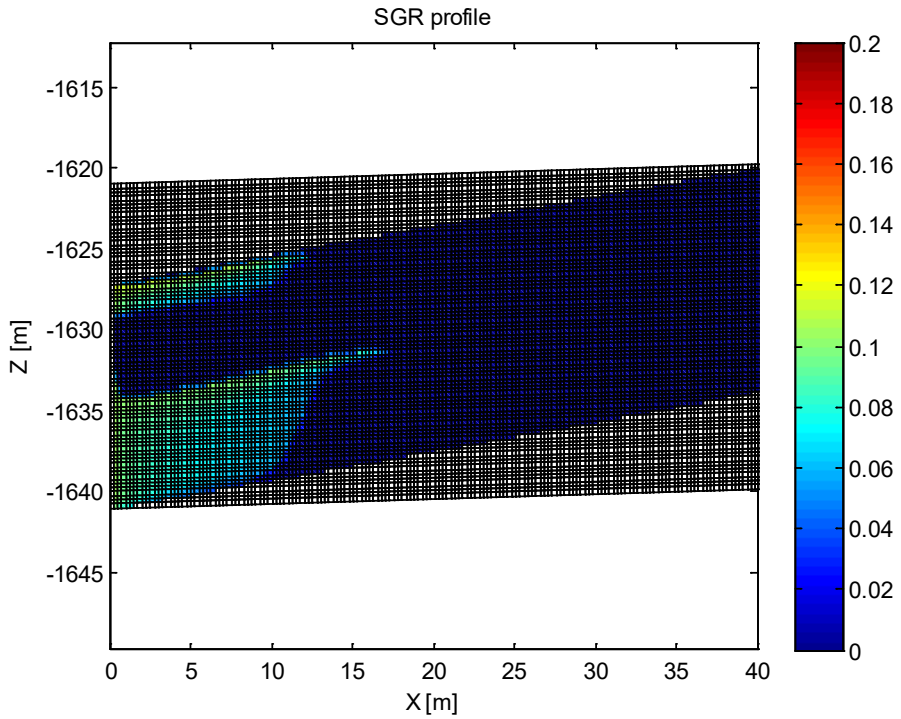


**Figure 6.9:** Residual "gas" saturation at time=10 days using the Aissaoui trapping model.

The trapping model was seen to be of major importance for the predicted residual trapping in the simulated scenario. At the end of observation (10 days) a difference in RTI of ca 0.3 (30% of injected $CO_2$ mass) was seen between the simulation results when using the modified Land/Jerauld trapping models compared to when using the Aissaoui trapping model (Figure 3). The same behavior was seen in simulated scenarios using 2D radially symmetric models (results not shown). The difference in residual trapping for the cases is due to the difference in trapping model (Figure 4.1) in the 0-0.4 $S_{gi}$ range.

## 6.2 **Impact of injection strategy on trapping**

The influence of different design components on the trapping is presented in the following subsections.

### 6.2.1 Effect of the amount of injected $CO_2$

The effect of the amount of injected $CO_2$ (250, 500, 750 or 1000 tons) on the trapping indexes was investigated, and are shown in Figure 6.10 to Figure 6.12. An injection rate of 1 kg/s was used in these simulations. Observe that the injection time is different between the cases. The saturation of $CO_2$-rich phase in the formation is shown in 6.13 and 6.14 for two different cases. The 2D radially symmetric model with DISC 2 was used. The amount of $CO_2$ injected has a large impact on the trapping indexes when observing trapping over a time period of 30 days. The residual trapping starts after the injection has ended, which gives the smaller amounts of injected $CO_2$ more time to redistribute and become trapped compared to when larger amounts of $CO_2$ is injected, and thereby a higher trapping efficiency for the smaller total amount injected.

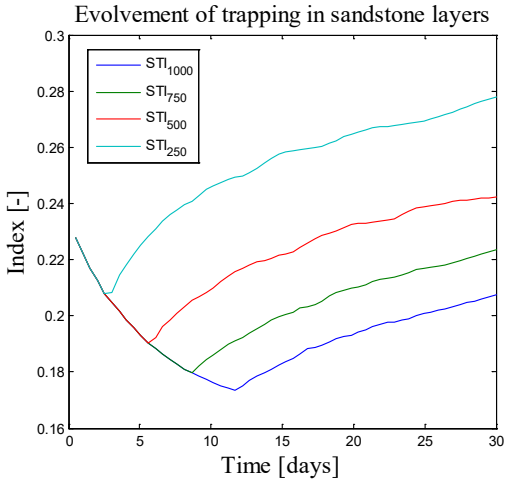


**Figure 6.10:** Solubility trapping index (STI) when injecting different amounts of $CO_2$.

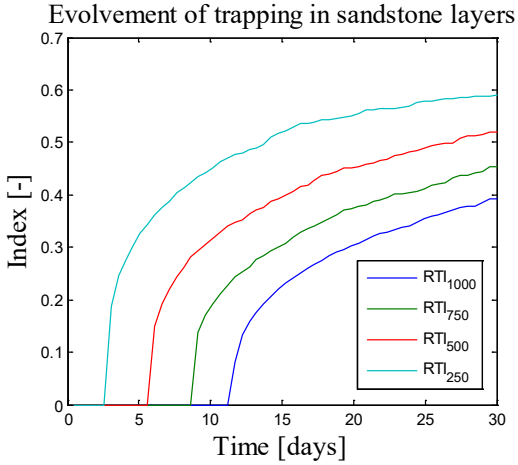


**Figure 6.11:** Residual trapping index (RTI) when injecting different amounts of $CO_2$.

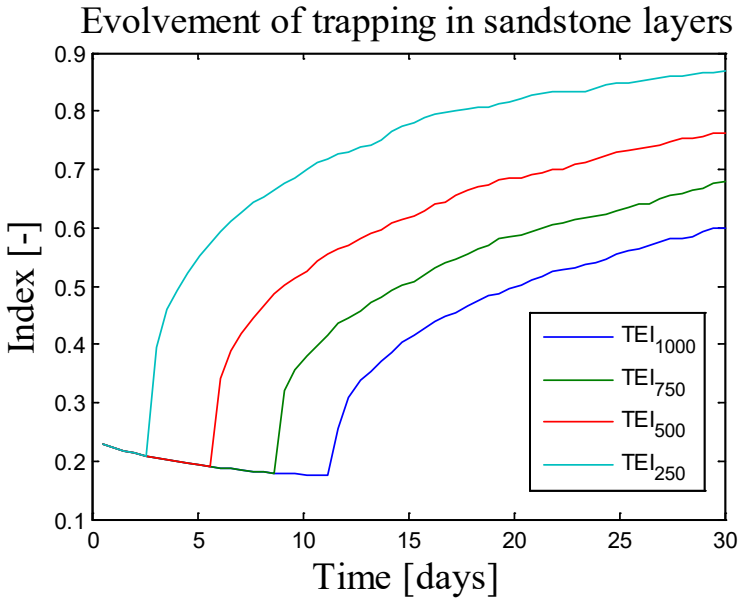


**Figure 6.12:** Trapping efficiency index (TEI) when injecting different amounts of $CO_2$.

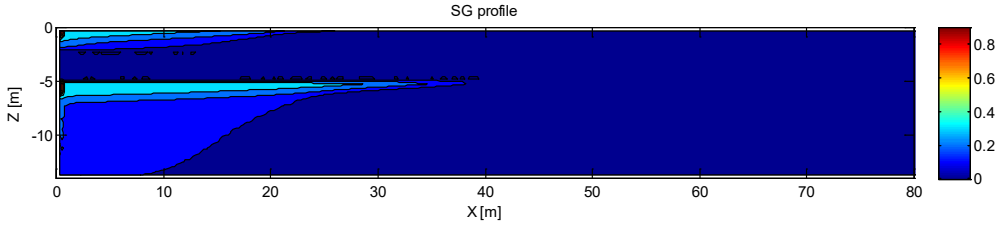


**Figure 6.13:** "Gas" saturation after 30 days from the start of injection for the case of in total 500 tons of $CO_2$ being injected at a rate of 1 kg/s.

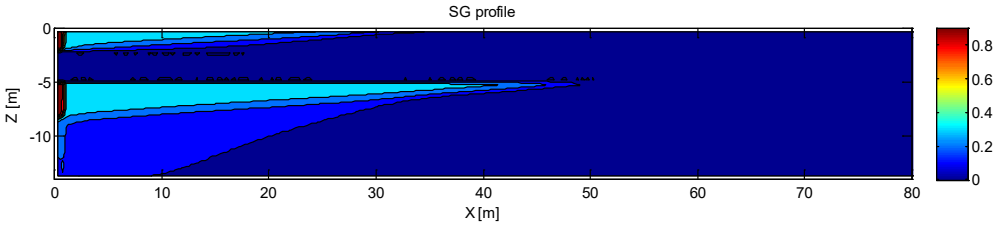


**Figure 6.14:** "Gas" saturation after 30 days from the start of injection for the case of in total 1000 tons of $CO_2$ being injected at a rate of 1 kg/s.

### 6.2.2 Effect of the injection rate of $CO_2$

The effect of the injection rate of $CO_2$ (0.3, 0.5, 0.6, 0.8 and 1 kg/s) on the trapping indexes was investigated, see Figures 6.15 to Figure 6.17. A 500 ton $CO_2$ injection was simulated and observations were made for 30 days from the start of injection.

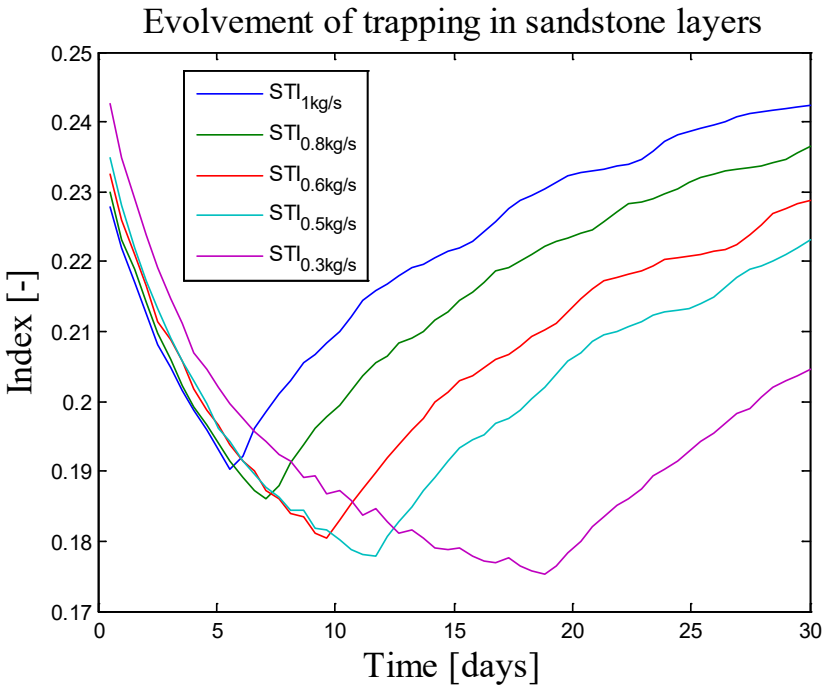


**Figure 6.15:** Solubility trapping index (STI) for cases with different injection rates of $CO_2$.

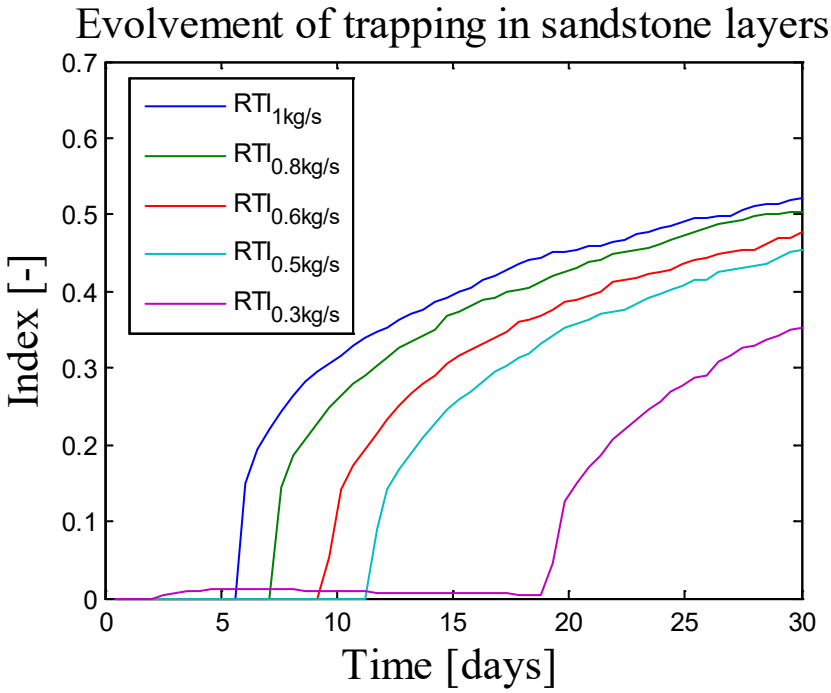


**Figure 6.16:** Residual trapping index (RTI) for cases with different injection rates of $CO_2$.

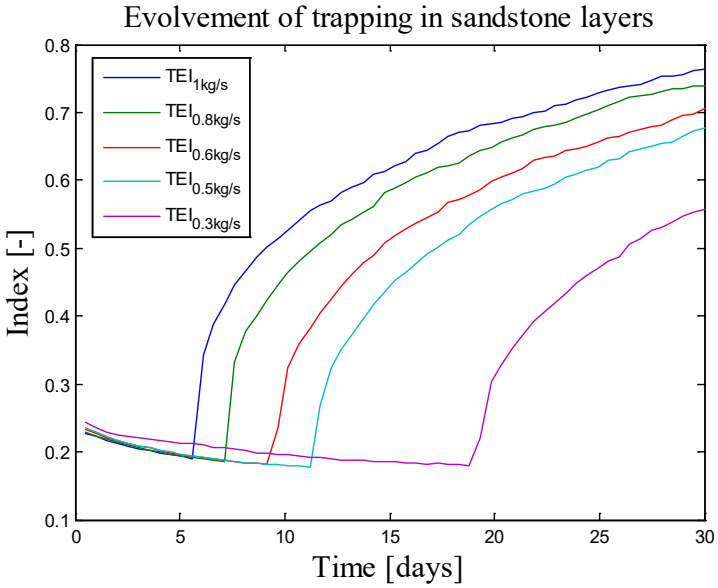


**Figure 6.17:** Trapping efficiency index (TEI) for cases with different injection rate of $CO_2$.

The results show that a higher injection rate corresponds to a longer redistribution time in-situ and consequently more residual trapping (when the same total time is considered is the redistribution time longer when injection time is shorter). It can also be seen that for the lowest injection rate some residual trapping starts before the end of injection as the rate is so low that buoyant migration occur also during the injection. This can be seen as the deviation of the purple line from zero, in Figure 5.16.

### 6.2.3 Effect of the amount of co-injected water

The effect of co-injection of water during the $CO_2$ injection (5, 10, 20 25, 30, 35 or 40 mass percent) on the trapping was investigated, see Figure 6.18 to Figure 6.20.

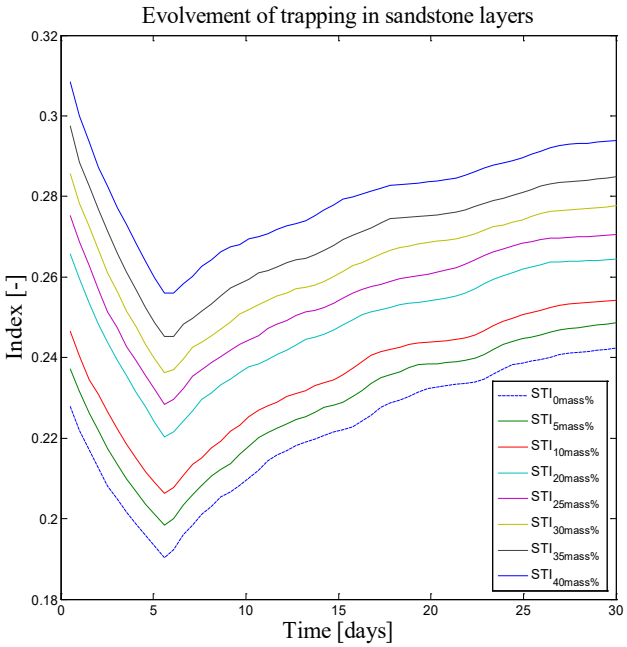


**Figure 6.18:** Solubility trapping index (STI) for different co-injection cases. The amount of water ranges from 0 to 40 mass percent.

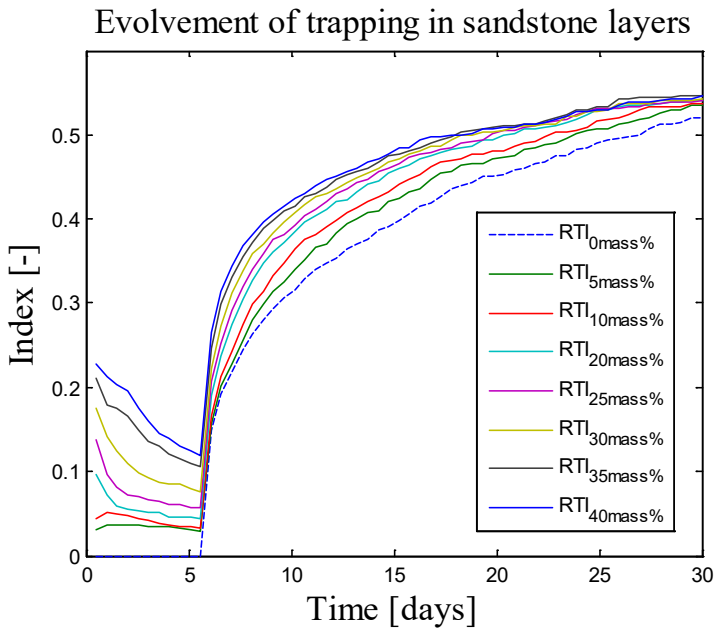


**Figure 6.19:** Residual trapping index (RTI) for different co-injection cases. The amount of water ranges from 0 to 40 mass percent.

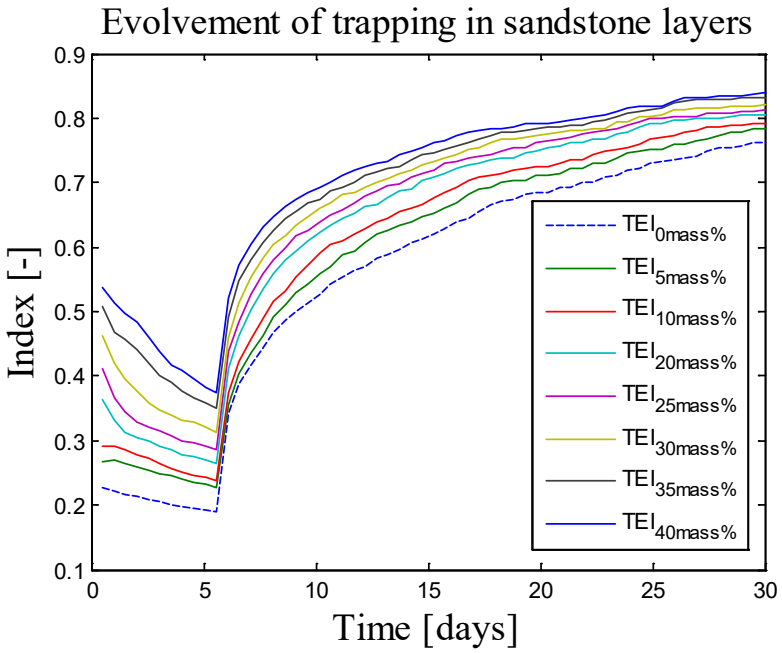


**Figure 6.20:** Trapping efficiency index (TEI) for different co-injection cases. The amount of water ranges from 0 to 40 mass percent.

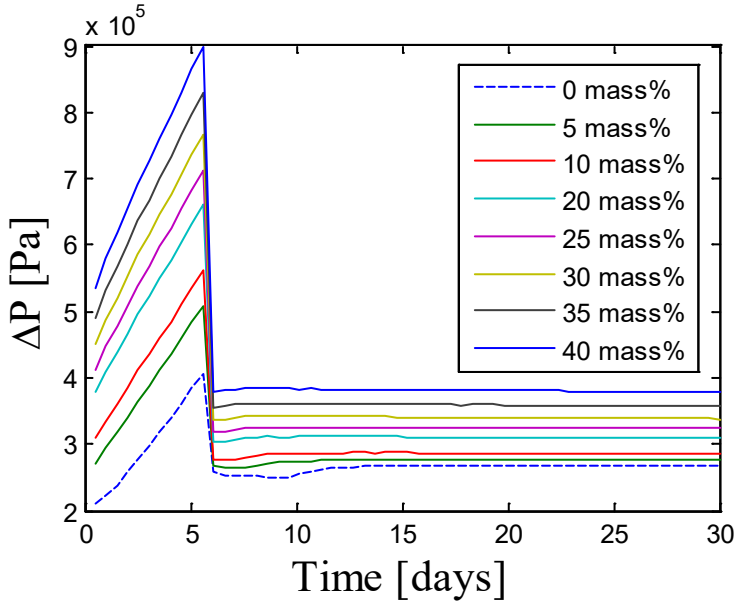


**Figure 6.21:** The pressure increase (ΔP) in the bottom of the well during 30 days. $P_{initial}$ was 1.47e7.

More trapping of $CO_2$ occurs during the injection stage when co-injection of water is employed, the effect being more pronounced the bigger the percentage of water is. The difference is however decreasing with time, especially due to the decreasing difference in residual trapping. As expected a larger mass percent of water does not only increase the residual and solubility trapping but also the injection induced pressure increase in-situ (Figure 6.21).

### 6.2.4 Effect of the amount of chase water

The effect of the quantity of chase water (water mass being 0, 15, 40 or 50 percent of the injected $CO_2$ mass), injected after a $CO_2$ injection was also investigated. A 500 ton $CO_2$ injection at a rate of 1 kg/s followed by a chase water injection at 1 kg/s was simulated. The impact on trapping indexes is shown in Figures 6.22 to 6.24 and the effect on bottom-hole pressure is shown in Figure 6.25. A larger amount of chase water corresponds to a longer injection time compared to a smaller amount of chase water.

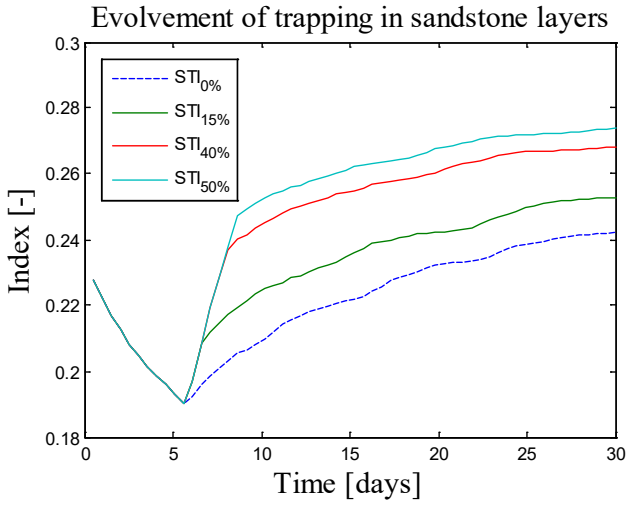


**Figure 6.22:** Solubility trapping index (STI) for scenarios with different quantities of chase water. The mass of chase water was 0, 15, 40 or 50 percent of the injected $CO_2$ mass.

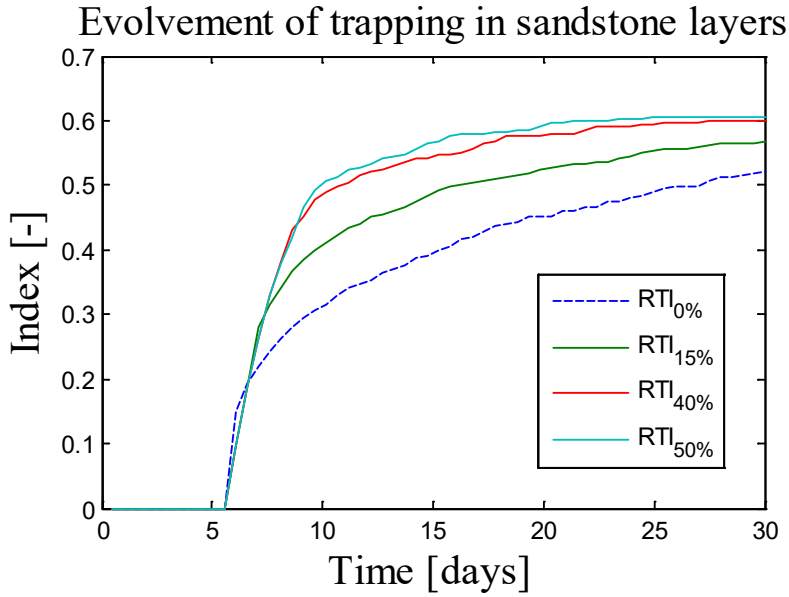


**Figure 6.23:** Residual trapping index (RTI) for scenarios with different quantities of chase water. The mass of chase water was 0, 15, 40 or 50 percent of the injected $CO_2$ mass.

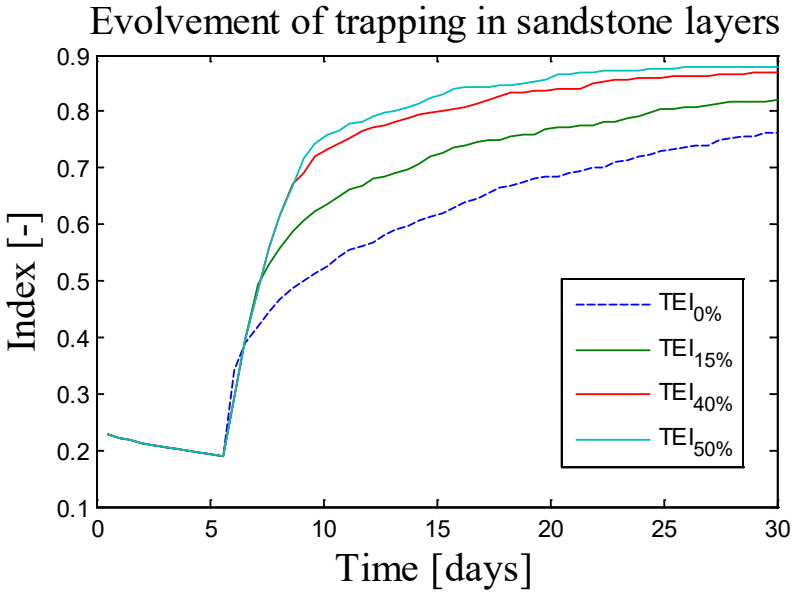


**Figure 6.24:** Trapping efficiency index (TEI) for scenarios with different quantities of chase water. The mass of chase water was 0, 15, 40 or 50 percent of the injected $CO_2$ mass.

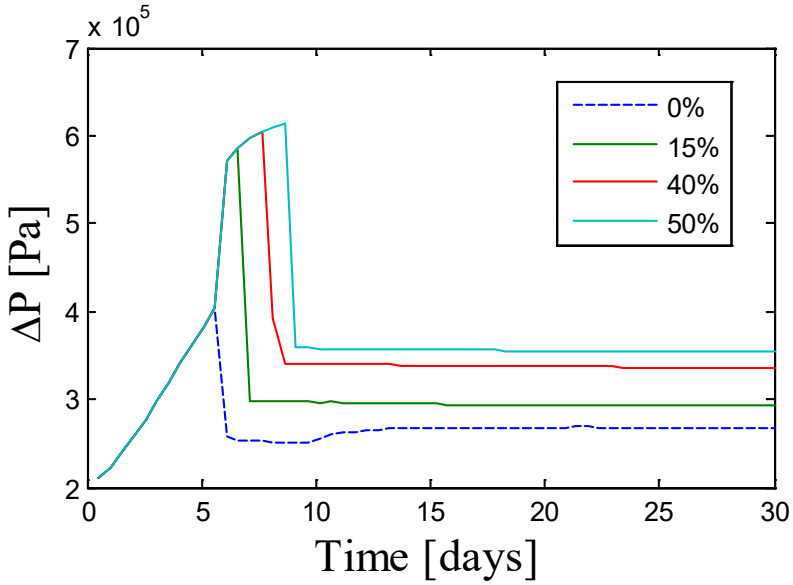


**Figure 6.25:** Pressure increase (ΔP) for scenarios with different quantities of chase water. The mass of chase water was 0, 15, 40 or 50 percent of the injected $CO_2$ mass.

The solubility trapping of $CO_2$ is increased by few percent when a chase water stage is included. The residual trapping is enhanced significantly during the actual chase water injection (Figure 6.23) this difference in residual trapping between cases where chase water have been used and the case without chase water is diminished with time and is less than 10 percent at the end of the observation period. Overall, the trapping index is systematically increasing with the increased total amount of the chase water. Injection of the chase water also results in a higher pressure (Figure 6.25). The peak in ΔP is seen to correspond to the time of the chase water injection.

### 6.2.5 Effect of the injection rate of chase water

The effect of the injection rate of the chase water (injected after a $CO_2$ injection) was also investigated. In this case a water mass of 15 percent of the injected $CO_2$ mass was used. The simulated scenario consisted of a 500-ton $CO_2$ injection at a rate of 1 kg/s, followed by a chase water injection at a rate of 0.25, 0.75 or 1 kg/s. Results can be seen in Figure 6.26 to Figure 6.29.

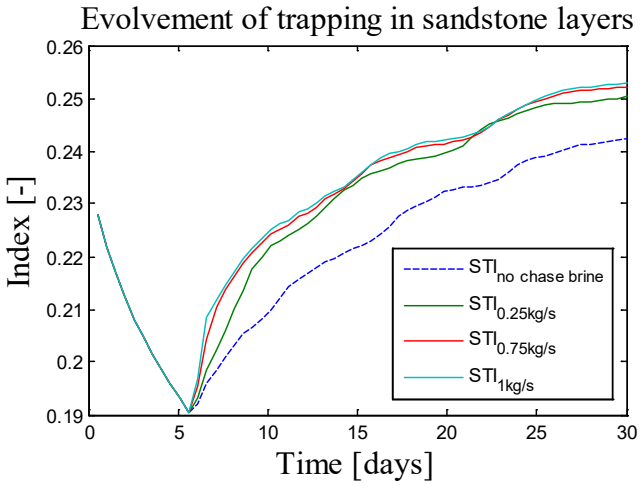


**Figure 2** Solubility trapping index (STI) for cases where different injection rates have been used for the chase water injection.

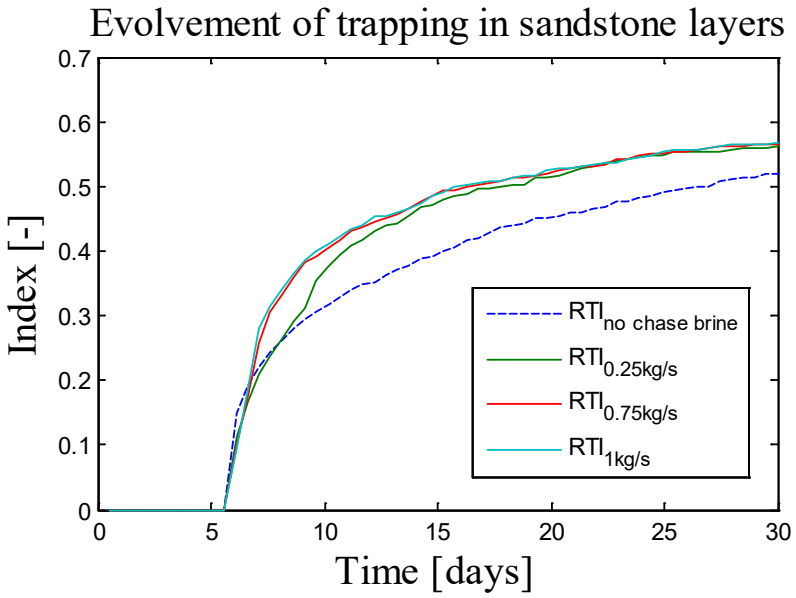


**Figure 6.27:** Residual trapping index (RTI) for cases where different injection rates have been used for the chase water injection.

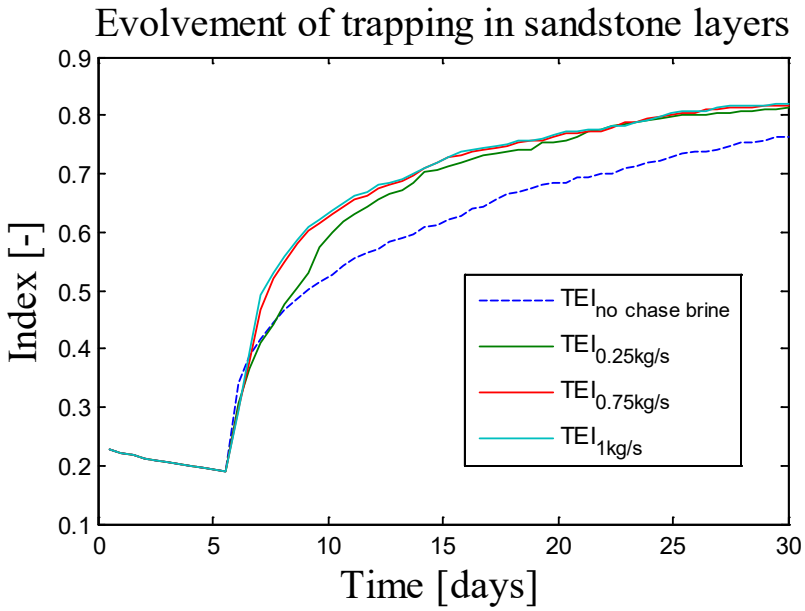


**Figure 6.28:** Trapping efficiency index (TEI) for cases where different injection rates have been used for the chase water injection.

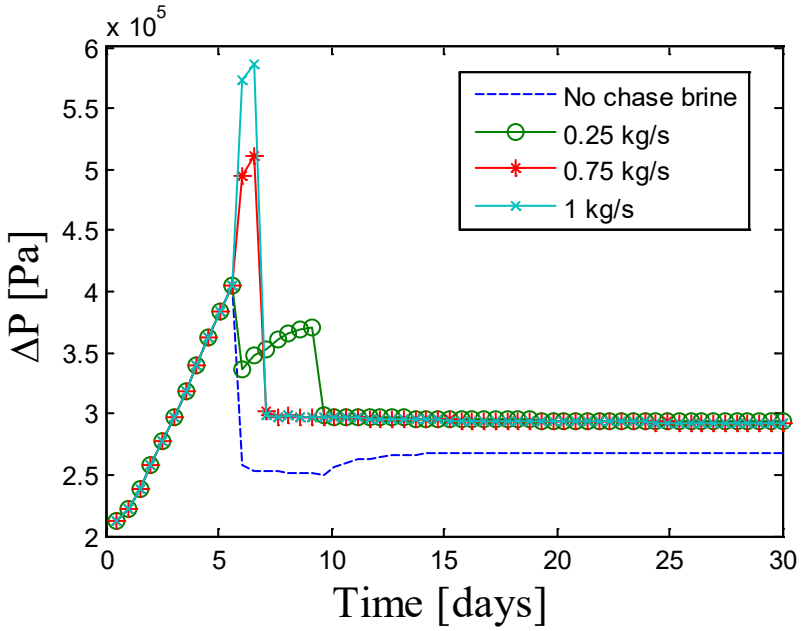


**Figure 6.29:** Pressure change (ΔP) for cases where different injection rates have been used for the chase water injection.

It can be seen that for this amount of chase water the injection rate has not much effect on the trapping (Figure 6.28), and the cases with different chase water injection rates are very similar to each other but different in comparison to the case without chase water injection. The pressure increase, however, is different for the different cases and the higher the chase water injection rate, the higher the pressure peak in the beginning (Figure 6.29).

### 6.2.5 Comparison of injection strategies

Comparison of the all six different injection strategies summarized in Table 2 is shown in Figure 6.30 to Figure 6.32. In these simulations the exact amounts and rates of injection for water and $CO_2$ given in Table 2 were used. The modified Land trapping model (standard) was used in all simulations.

When comparing the trapping for the different injection strategies a maximum difference of 0.12 in the TEI (Figure 32) is seen at day 30 from the start of injection. At day 30 of observation all strategies except the cyclic injection have enhanced the trapping in comparison to the conventional case, mainly through increased residual trapping. Cyclic injection, as well as the WAG injection strategies, can greatly increase residual trapping on a shorter time perspective (compared to conventional injection at e.g. day 4). Overall, the mixed co-injection combined with chased injection and the chased injection provide the best overall trapping. The different injection strategies also resulted in different pressure responses. The pressure increased most for strategies which combined injection of both water and $CO_2$. Figure 6.32 shows the residually trapped $CO_2$ in the formation resulting from the different injection strategies. When employing strategies consisting of chase water injections (strategy 2, 4 or 6), residually trapped $CO_2$ is lacking in the vicinity of the well due to dissolution into the liquid phase.

When comparing the trapping for the different injection strategies a maximum difference of 0.12 in the TEI (Figure 6.30) is seen at day 30 from the start of injection. At day 30 of observation all strategies except the cyclic injection have enhanced the trapping in comparison to the conventional case, mainly through increased residual trapping. Cyclic injection, as well as the WAG injection strategies, can greatly increase residual trapping on a shorter time perspective (compared to conventional injection at e.g. day 4). Overall, the mixed co-injection combined with chased injection and the chased injection provide the best overall trapping. The different injection strategies also resulted in different pressure responses. The pressure increased most for strategies which combined injection of both water and $CO_2$. Figure 6.32 shows the residually trapped $CO_2$ in the formation resulting from the different injection strategies. When employing strategies consisting of chase water injections (strategy 2, 4 or 6), residually trapped $CO_2$ is lacking in the vicinity of the well due to dissolution into the liquid phase.

(a)

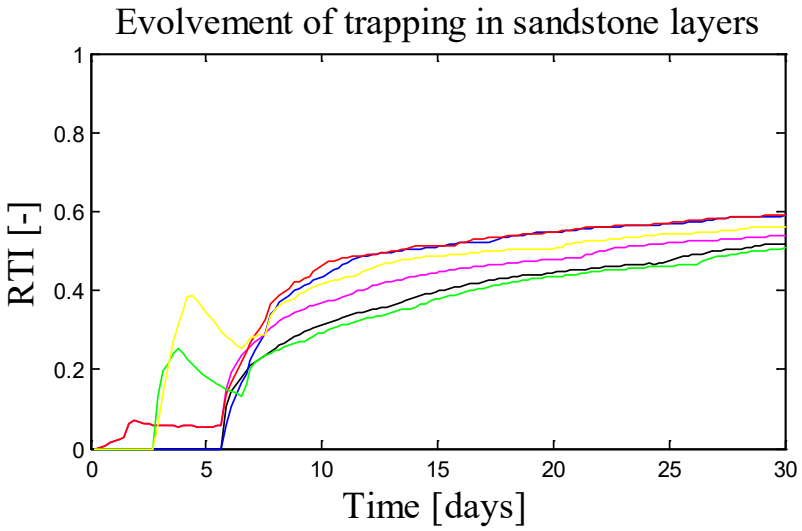


(b)

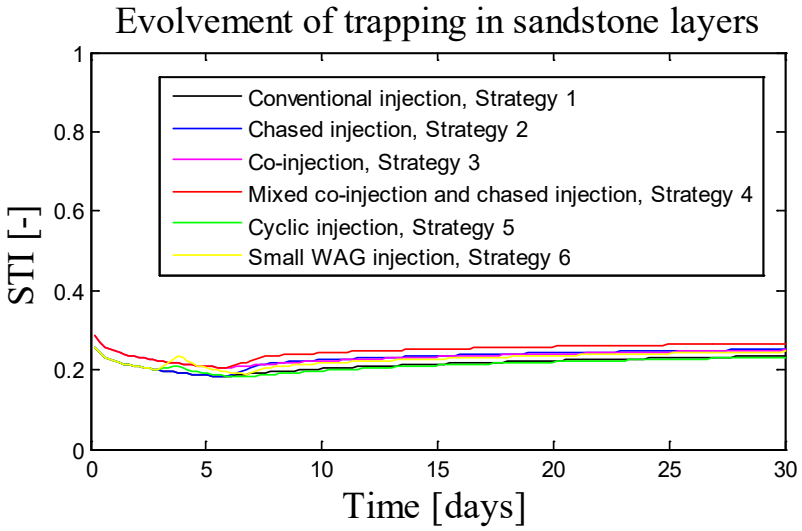


(c)

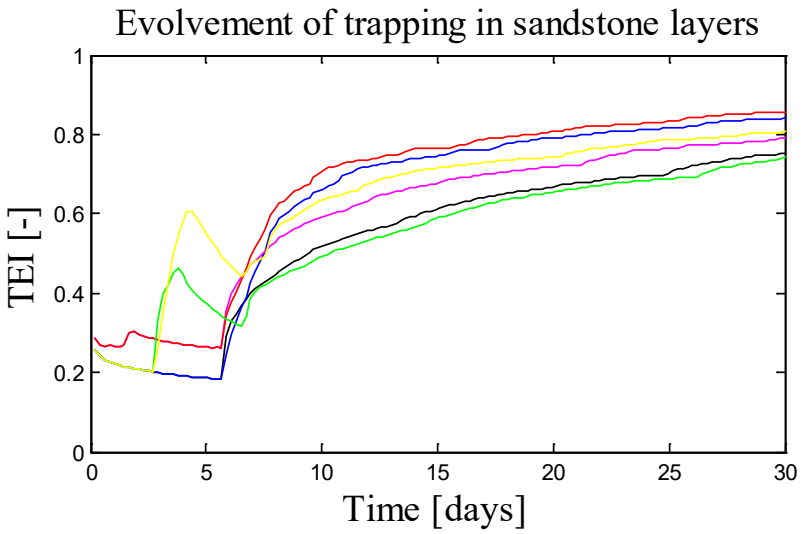


**Figure 6.30:** (a) - Residual trapping index (RTI), (b) - Solubility trapping index (STI) and (c) - Trapping efficiency index (TEI) for different injection strategies.

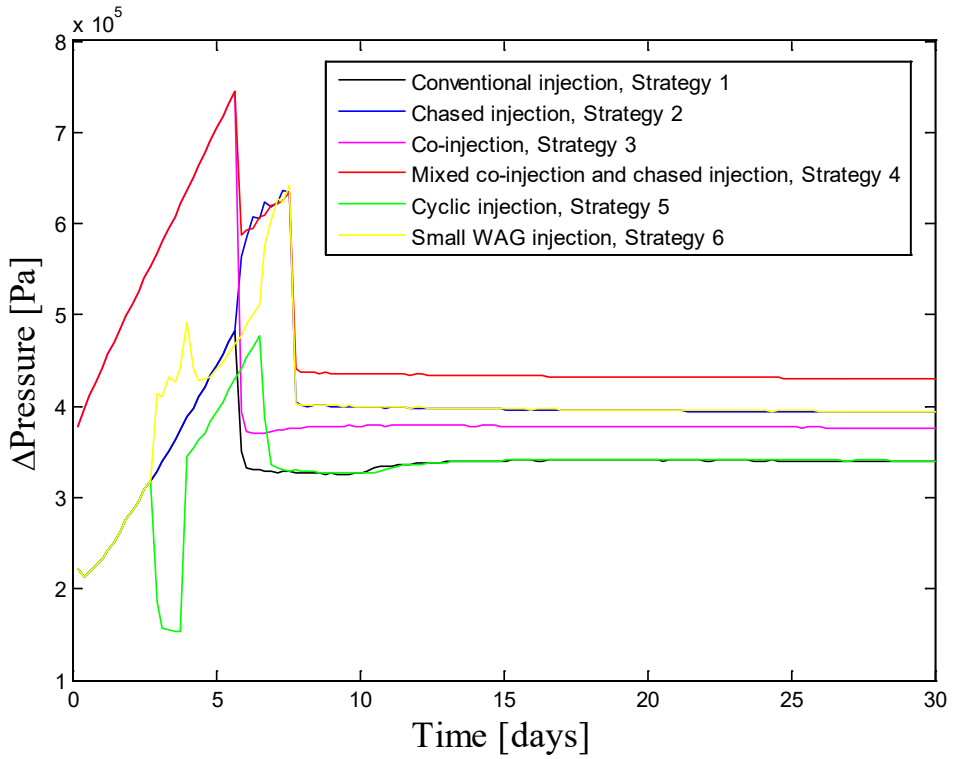


**Figure 6.31:** Pressure change (ΔP) in well bottom for different injection strategies.

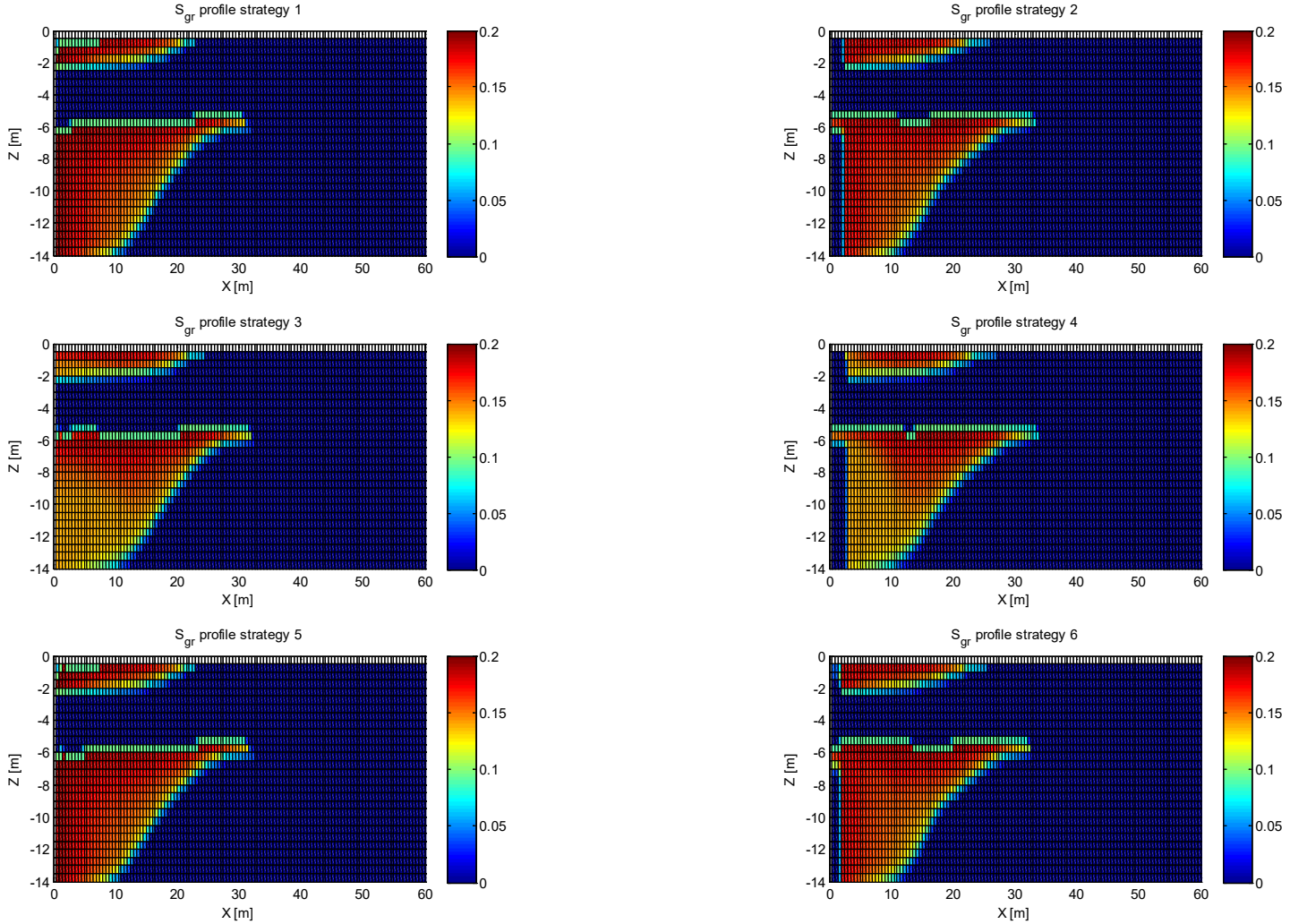


**Figure 6.32**: Residually trapped "gas" saturation in the formation at day 30 for the different injection strategies. Observe that the scale in the x-direction differs from the scale in the z-direction.

## 6.3 **Impact of geological heterogeneity on trapping**

The impact of geological heterogeneity (permeability and porosity) on trapping was also studied, in order to relate that to the differences observed due to the injection strategy studied in previous chapter. 6.33 and 6.34 show one of the k-field realizations and corresponding $CO_2$ plume at the end of the observation period of 30 days.

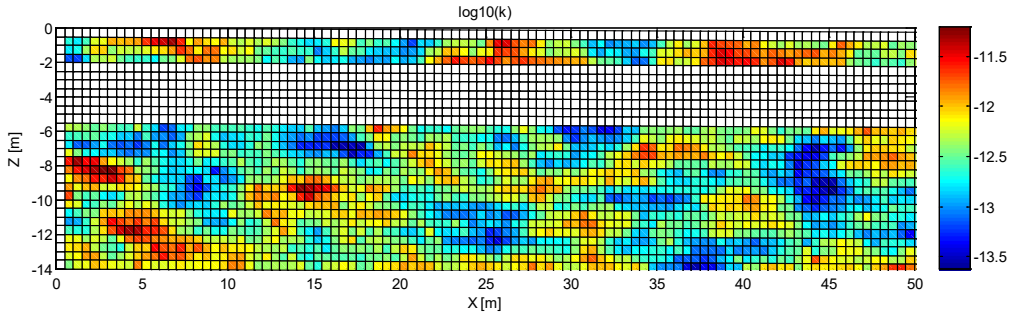


**Figure 6.33:** Heterogenous k-field realization. The model is 500 m in radius and the heterogeneity applied to the inner 50 m.

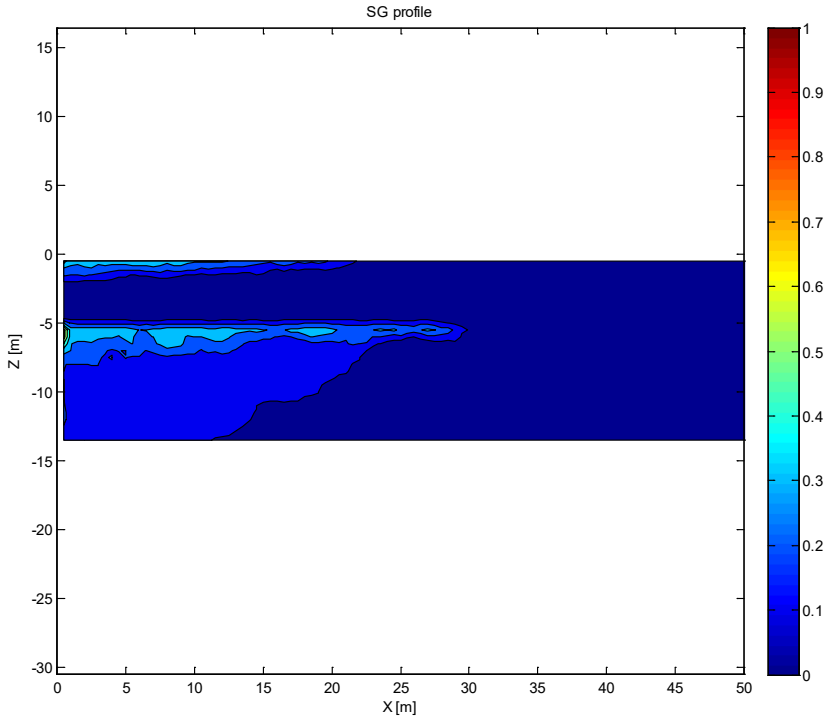


**Figure 6.34:** "Gas" saturation at day 30 for the k-field shown in the figure above.

The simulated scenario was the "conventional injection strategy", see Table 2. 500 tons of $CO_2$ was injected at a rate of 1 kg/s and the trapping in the formation was observed for 30 days from the start of injection. The standard modified Land trapping model was used. The results shown in 6.35 to 6.37 are based on 34 realizations. The results of the heterogeneous realizations are shown as box-and-whiskers plots (the central 50% corresponding to the blue box) and for comparison, the homogeneous case is shown with the solid black line. The 2D radially symmetric model with DISC 1 was used in these simulations.

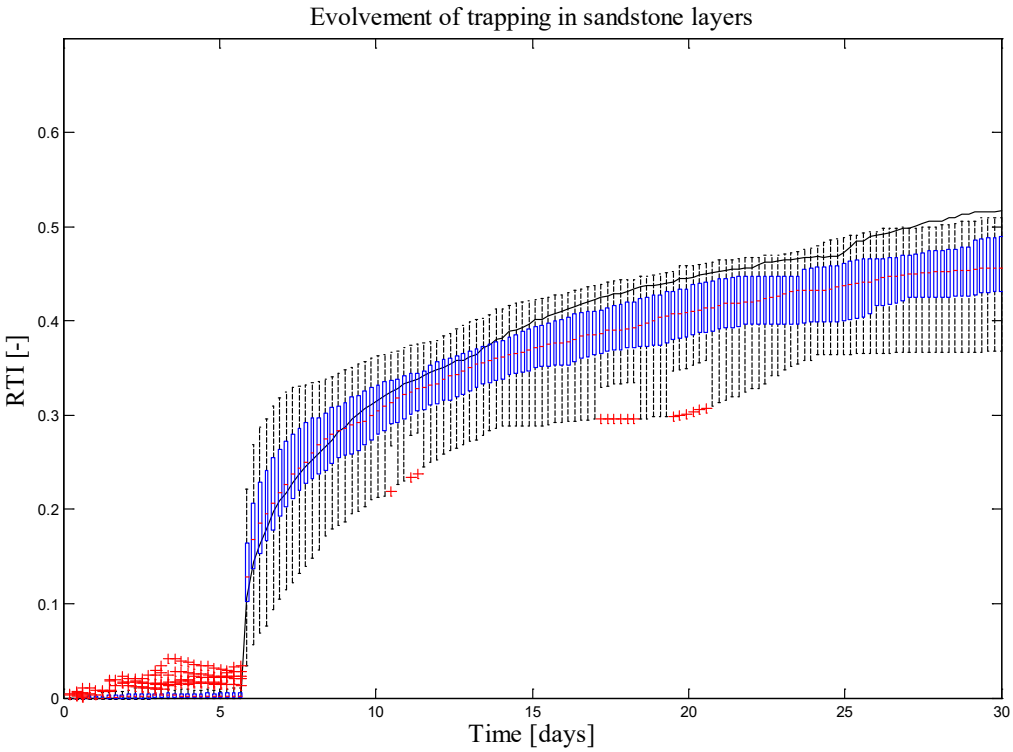


**Figure 6.35:** Residual trapping index (RTI) for the homogeneous case (black line) and heterogeneous case (represented by box plots).

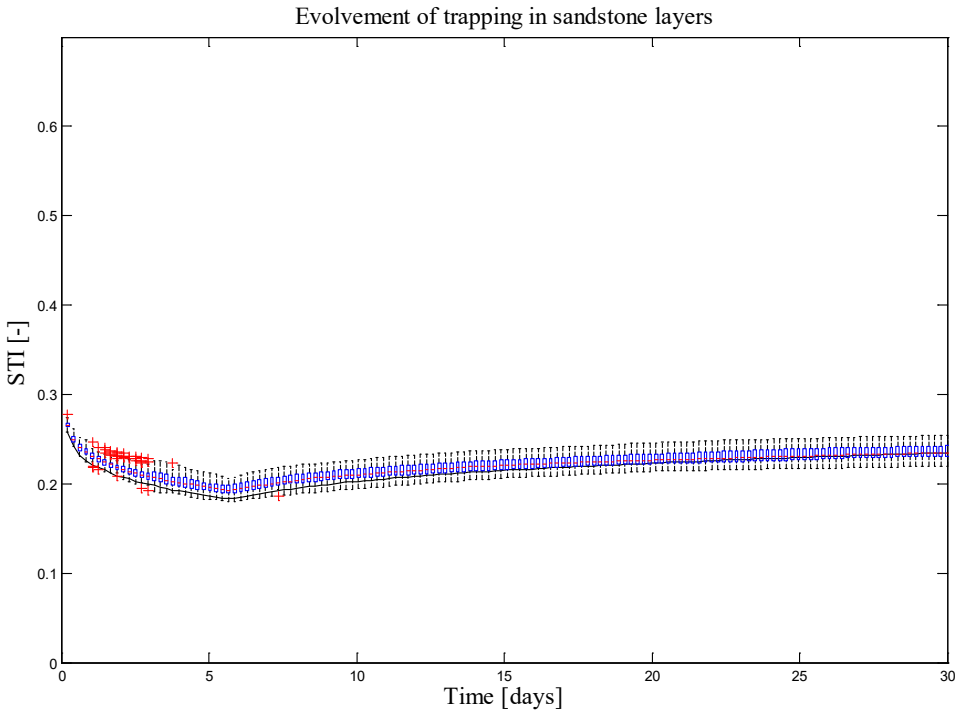


**Figure 6.36:** Solubility trapping index (STI) for the homogeneous case (black line) and heterogeneous case (represented by box plots).

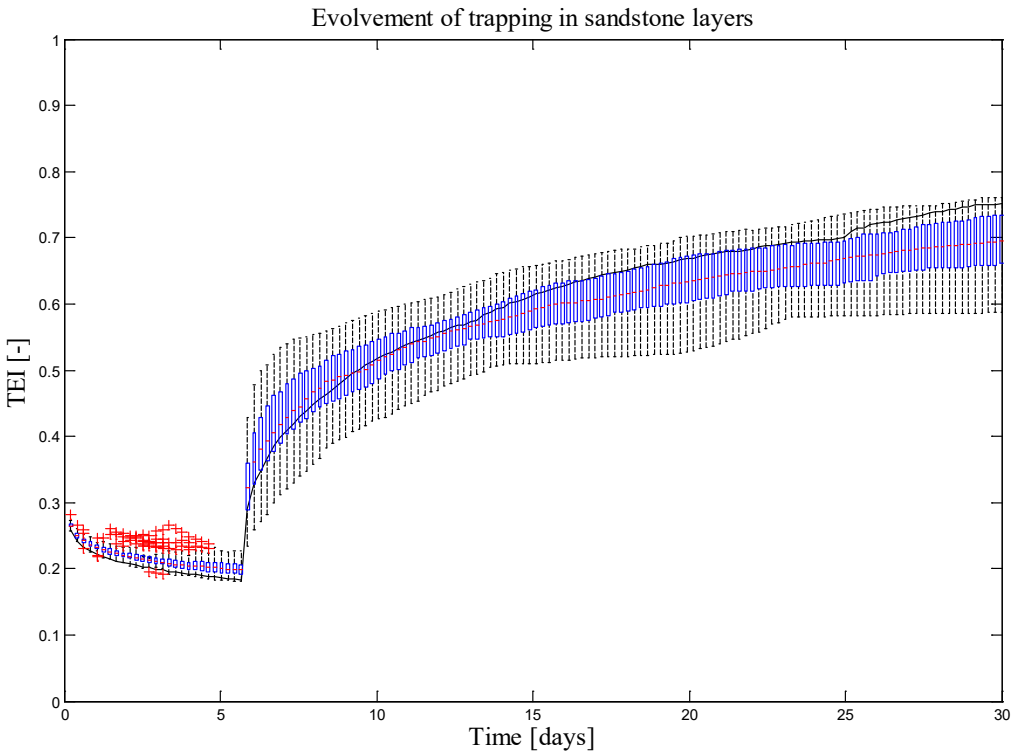


**Figure 6.37:** Trapping efficiency index (TEI) for the homogeneous case (black line) and heterogeneous case (represented by box plots).

It can be seen that short after the injection ends the trapping in the heterogeneous case (median TEI) is higher than for the homogeneous case. At the later times, however, the trapping becomes higher for the homogeneous case in comparison to most of the heterogeneous realizations. This is due to the fact that on longer time scales, heterogeneity is retarding the buoyant migration which results in less imbibition and thereby less residually trapped $CO_2$.

# 7. 3D simulations

The previous simulations were carried out with simplified geometries of the complex 3D reality, namely a 2D slice with dip and a 2D radially symmetric model. This is as the full 3D model is highly computationally intensive and the simplified models allowed inspection of a wider range of injection strategies and phenomena. In the following we will investigate the system with fully 3D model, including heterogeneity, in some specific cases.

## 7.1 Conceptual model and numerical simulations

The (half-space) conceptual model which includes two sandstone layers (2 and 9 m thick) and an intermediate shale layer (3m thick) is shown in Figure 7.1. The angle of the formation is 7.7 degrees and layers are assumed to be parallel. There is one injection and one observation well 40m apart, based on the information from the Heletz site. Formation properties are summarized in Table 7.1 in which sandstones A and W are assigned the same petrophysical properties.

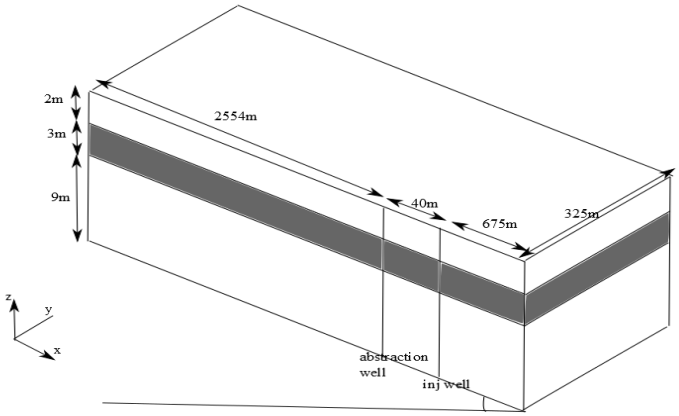


**Figure 7.1:** The conceptual model

To generate an unstructured 3D mesh, Petrasim software was used (a schematic view of the mesh close to the wells is shown in Figure 7.2. TOUGH2-EOS7C model was used for the simulations. To generate the heterogeneity field between wells, Gslib (SGSIM) model was applied. Correlation length in vertical direction is 2.7m and variance has been varied (0.2, 0.4, 0.5). It should be noted that heterogeneity is only applied between the wells and within sandstone layers while the rest of the domain is assumed homogeneous. Relative permeability function and capillary pressure are according to Brooks-Corey model and boundaries are no-flow everywhere.

The parameter that was compared between different models is dissolution index (DI) which is defined as a proportion of aqueous phase $CO_2$ and total amount of injected $CO_2$ at the time. The realizations of three permeability fields are shown in Figure 7.3. A cycle of one day of $CO_2$ injection followed by one day of water injection was simulated. The total amount of injected $CO_2$ was 100 tons (since the simulations have been carried out for half space, because of symmetry, the amount of injected $CO_2$ is 50 tons) and the total amount of the injected water is 200 tons (twice of that of $CO_2$).

**Table 7.1:** Formation parameters and initial conditions

| Parameter | Value |
|---|---|
| *Sandstone* | |
| Grain density [g/cc] | 2645 |

| | |
|---|---|
| Porosity [-] | 0.25 |
| Absolute permeability [mD or $m^2$] | 730 |
| Pore compressibility [$Pa^{-1}$] | 4.5e-10 |
| Residual gas saturation | 0.2 |
| Residual water saturation | 0.3 |

*Shale*

| | |
|---|---|
| Grain density [g/cc] | 2555 |
| Porosity [-] | 0.06 |
| Absolute permeability [mD or $m^2$] | impermeable |
| Pore compressibility [$Pa^{-1}$] | 4.5e-10 |
| Residual gas saturation | 0.2 |
| Residual water saturation | 0.3 |

*Initial conditions*

| | |
|---|---|
| Temperature [ºC] | 60 |
| Salinity [salt mass fraction] | 0.05 |
| Pressure [Pa] at the bottom of the formation | 1.47e7 |
| Formation salinity | 52502 mg/L |
| Gravitational acceleration vector [$m/s^2$] | 9.81 |

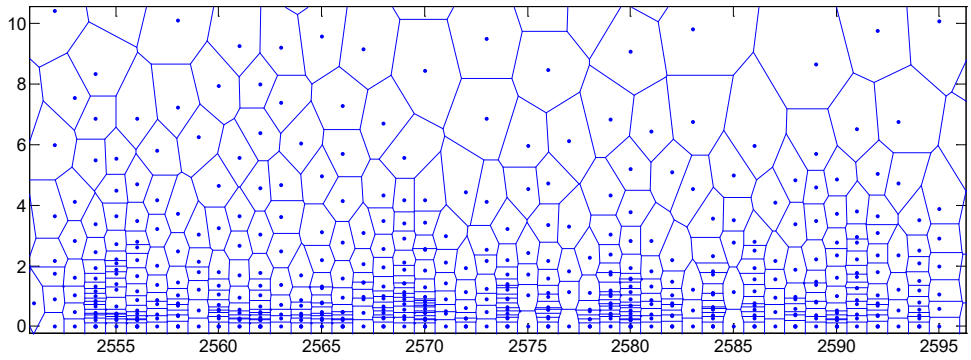


**Figure 7.2:** Schematic top horizontal view of the mesh (XY plane) around the wells

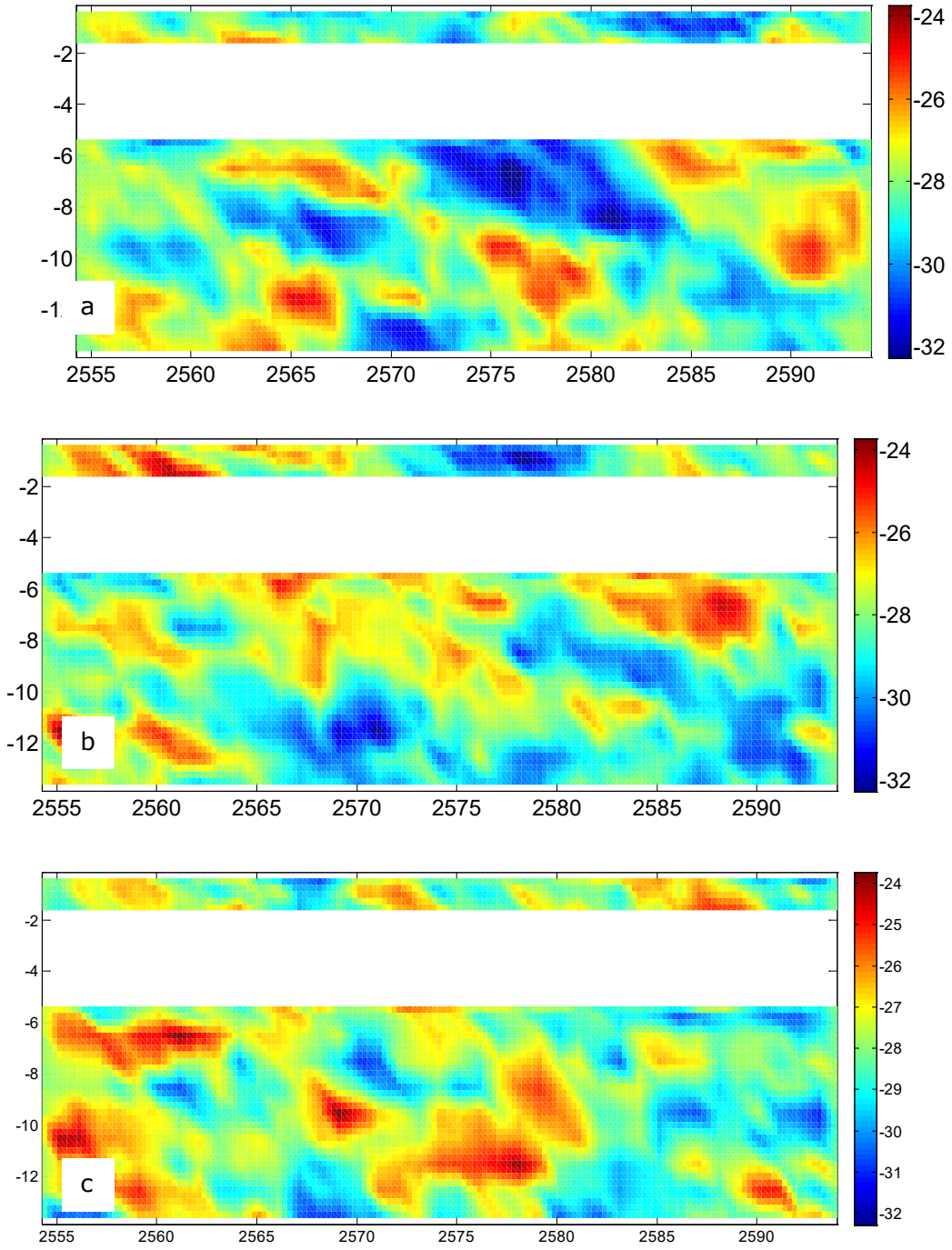


**Figure 7.3:** Different permeability realizations generated using Gslib for sill value of 0.5 and correlation length of 2.7m in vertical direction (please recognize that inclined appearance of the heterogeneity is due to the different scales in x and y)

## 7.2 **Effects of different injection scenarios**

To test the effect of permeability field, the three realizations above have been compared for a scenario of two cycles of injection i.e. one day gas injection followed by one day of water injection repeatedly, with total injection rate of 2 ton/hour (1 ton/hour for half space). Gas saturation profiles after 10 days for these simulations are shown in Figure 43. A 3D plot of $CO_2$ plume expansion after 10 days for the same scenario with permeability field "a" is shown in Figure 45.

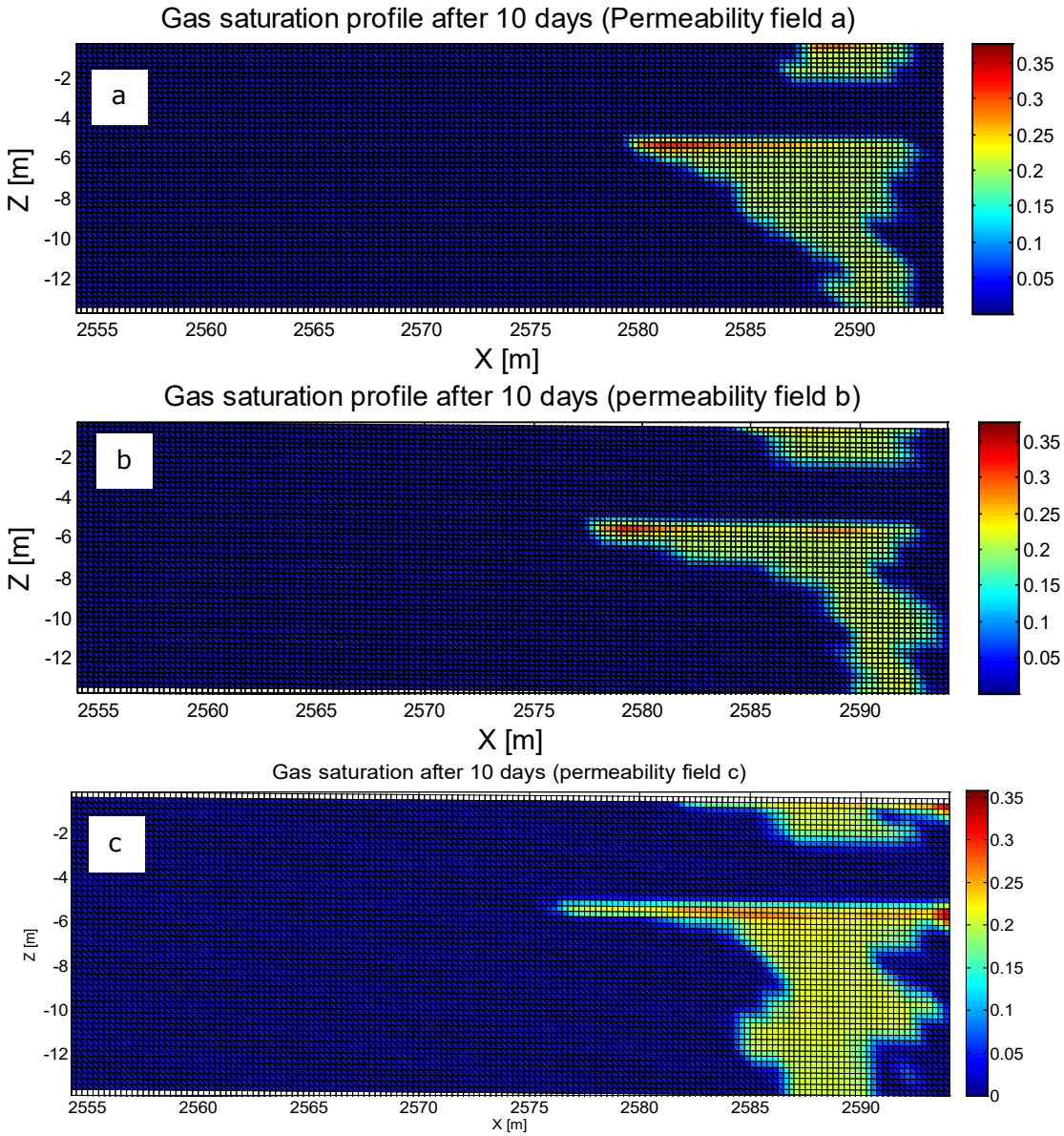


**Figure 7.4:** Gas saturation profile after 10 days for different permeability fields.

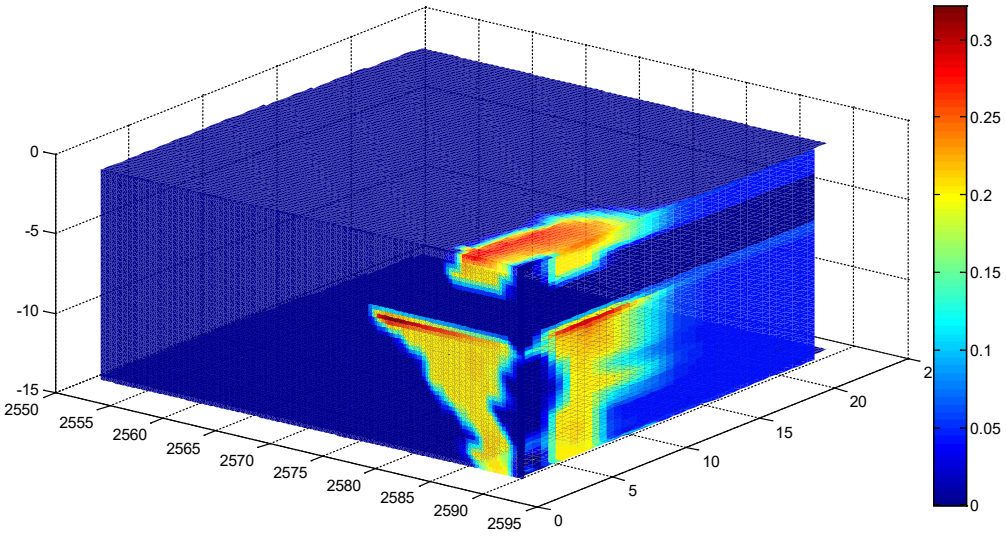


**Figure 7.5:** 3D plot of gas saturation after 10 days for the scenario of two cycles injection with heterogeneity field "a" (one day gas injection following by one day water injection repeatedly with total injection rate of 2 ton/hour (1 ton/hour for half scape)).

For all the following simulations, permeability field "a" has been used.

### 7.2.1 The effect of water alternating gas (WAG) (permeability field 'a')

To test the effect of alternating $CO_2$ and water injection, dissolution index is compared between cases with only $CO_2$ injection and one with $CO_2$ injection following by water injection. The result is shown in Figure 7.6. It can be seen that water alternating $CO_2$ will increase the dissolution index.

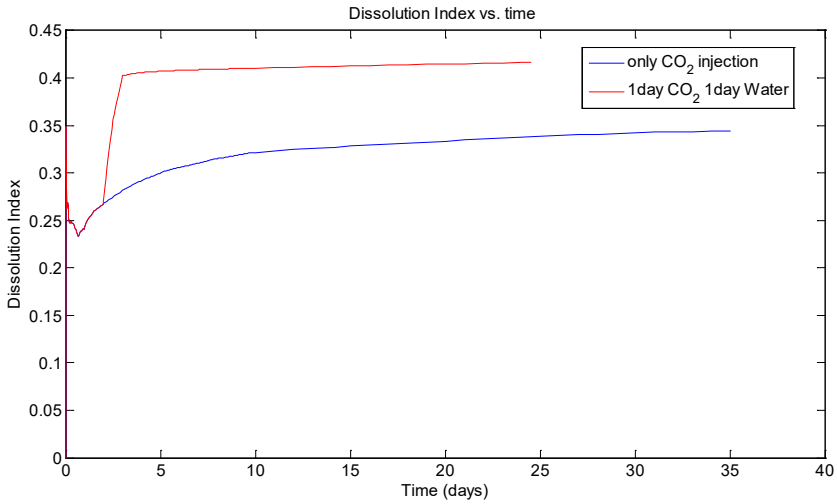


**Figure 7.6:** Comparing dissolution index for cases of one day $CO_2$ injection and one day $CO_2$ injection following by one day water injection.

### 7.2.2 The effect of the injection rate

A change in injection rate can affect the dissolution index. Two different $CO_2$ injection rates (2 and 4 tons per hour) were tested in a one-cycle injection and the result is shown in Figure 7.7. Higher $CO_2$ injection rate will in principle increase the pressure at the vicinity of the injection well and will dominate the gravity effect and make it easier for the gas to overcome the entry pressure of the pores whereas in the case of lower injection rate, gas plume will tend to follow the high permeable paths. This effect is however very small in the case of Figure 7.7. When injection is performed in cycles, we see a more pronounced effect (Figure 7.8), where the injection is carried out in more than one cycle but the total amount of injected fluids is kept constant. It can be seen that highest dissolution is achieved with the single cycle where the injection rate is highest. The effect of higher injection rate on dissolution was already seen in the simulations presented in section 6.2.2.

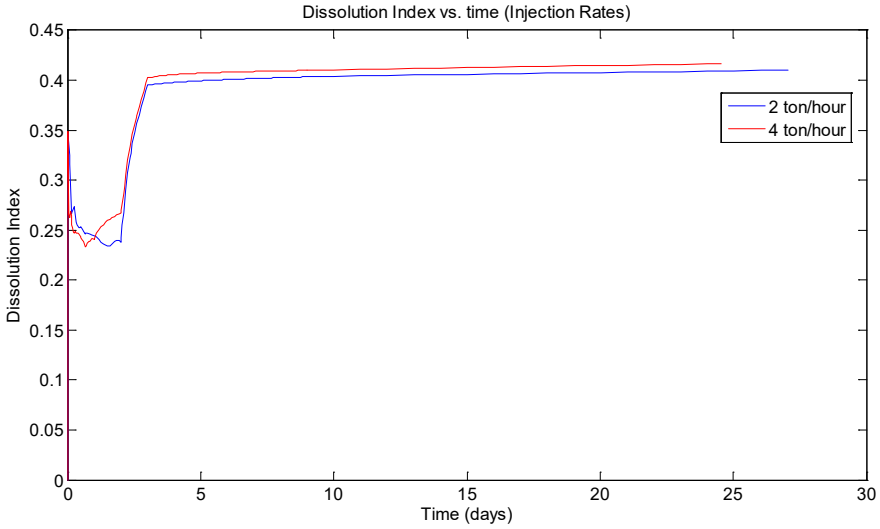


**Figure 3:** Comparison of dissolution index for two different CO2 injection rates.

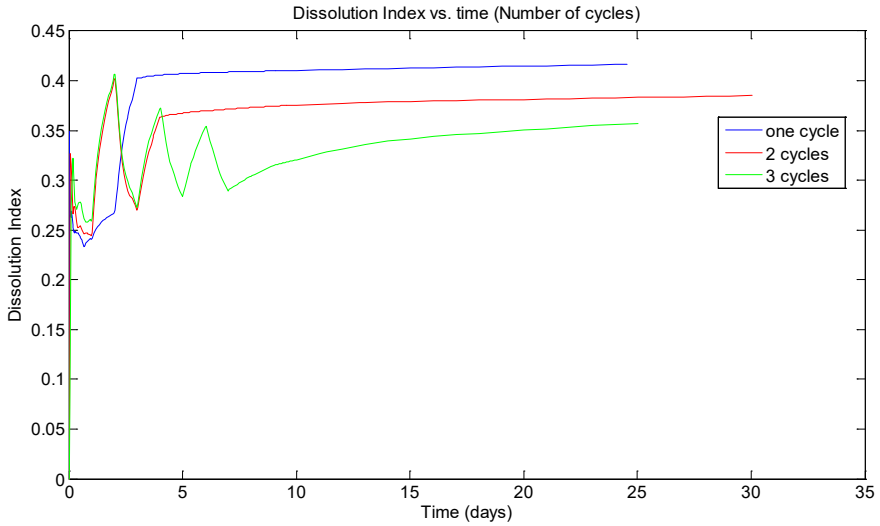


**Figure 7.8:** Dissolution index vs. time for scenarios with different number of cycles.

### 7.2.3 Heterogeneity effects

Figure 7.9 illustrates the effect of heterogeneity on the dissolution index. As it is shown the dissolution will increase with increasing level of heterogeneity (increase in variance) and homogeneous case has the lowest dissolution index. This is somewhat contradictory to the results with two-dimensional simulations where the homogeneous case fell in the middle of the heterogeneous cases for dissolution trapping (and where heterogeneity had a decreasing effect on residual trapping). The explanation may be that in three-dimensions more possibilities for by-passing low-permeability zones exists.

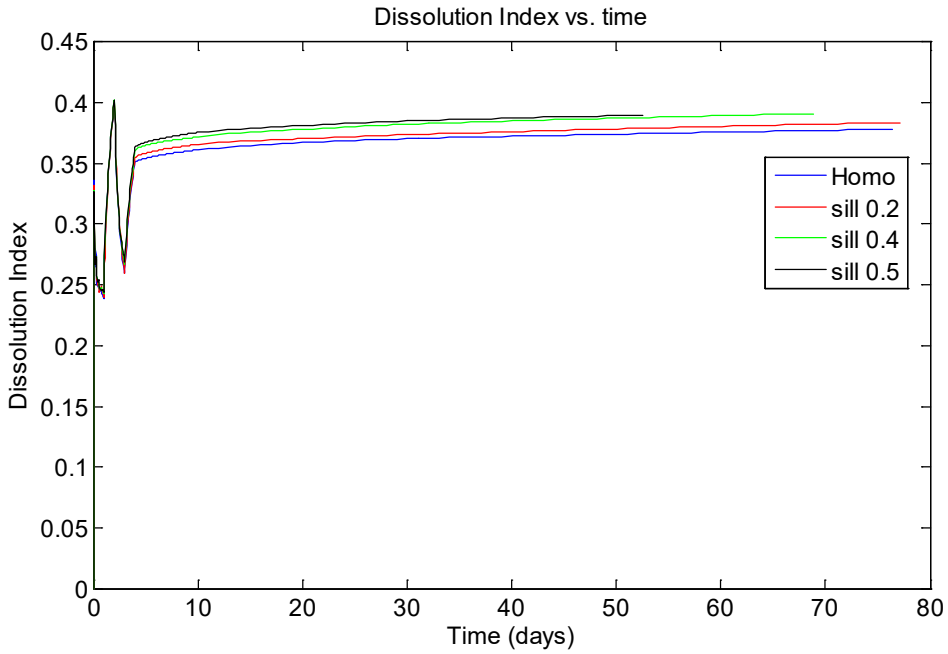


**Figure 7.9**: The effect of heterogeneity on dissolution index.

### 7.2.4 The effect of abstraction in the monitoring well

For a scenario with two injection cycles, the effect of continuous abstraction in the second well (monitoring well in Heletz setting) was tested. This is as abstraction may be necessary for the practical water supply for carrying out the experiment. Figure 7.10 shows the increase in dissolution index when there is continuous pumping during the whole simulation time from the second well 40 m away from the injection well. The reason might be due to the effect of pumping expanding the plume. The larger $CO_2$ front can increase the interface of gas and water and as a result it can increase the dissolution.

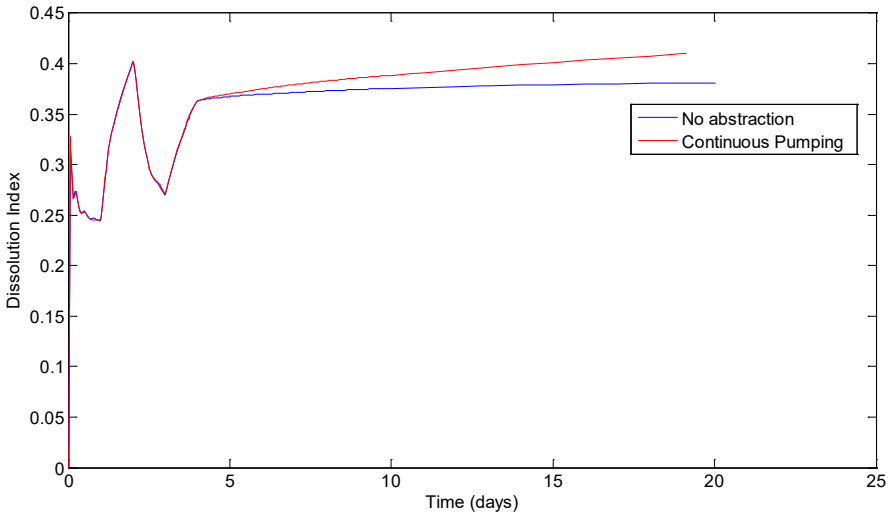


**Figure 7.10:** The effect of continuous water abstraction from the second well

### 7.2.5 The effect of adding rest periods

Figure 7.11 compares two simulations of two cycles where one of them has a rest day after each $CO_2$ injection phase. In other words, a cycle of $CO_2$ injection/water injection (CW) is replaced with a cycle of $CO_2$ injection/rest period/water injection (CRW). It can be seen that dissolution index has increased for the scenario with a rest day after $CO_2$ injection. The effect is quite insignificant for the homogeneous case but more obvious when heterogeneity exists. The reason again can be related to the larger interface, since in the case with a rest day after $CO_2$ injection, $CO_2$ plume has more time to move forward.

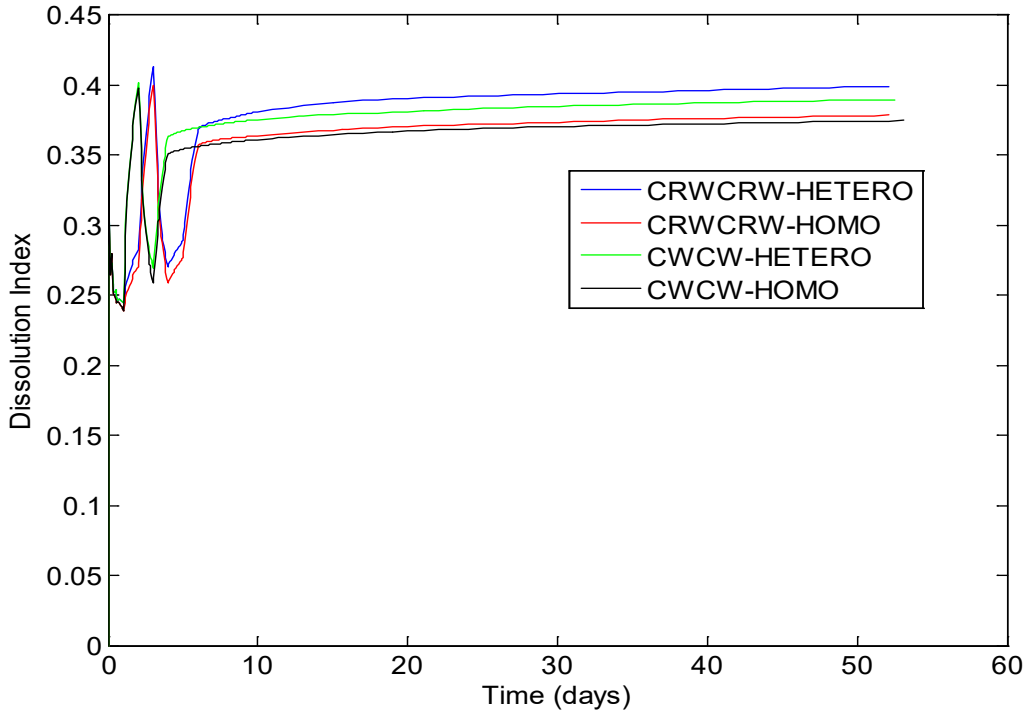


**Figure 7.11:** Comparison of dissolution index between two 2-cycles scenarios, while one cycle has a rest day after $CO_2$ injection.

# 8. Conclusions

In this work we carried out a comprehensive set of simulations to investigate the effect of different modes of injection to enhance trapping, with the objective to provide design guidance to Heletz $CO_2$ injection experiments in TRUST project.

Effect of varying various design parameters was evaluated as were a number of different injection strategies. Effect of geological heterogeneity was considered as well.

To allow a large number of scenarios to be considered vertical models with radial symmetry were first considered, including multiple realization heterogeneous simulations. From these simulations both the residual and dissolution trapping were determined and the results were compared by looking at the various trapping indices (trapped amount of $CO_2$ in relation to the total amount of injected $CO_2$). These were followed by a more limited number of full three-dimensional simulations focusing on dissolution trapping only. In all simulations total amounts and injection rates were selected according to the specifications of the Heletz site, i.e. a small-scale pilot test.

Firstly, it was observed that the accuracy of the trapping model used for describing residual trapping is of major importance for the predicted residual trapping. The difference in predicted residual trapping arising from the use of different trapping model was of the order of 0-0.4.

Second, the effect of both the total amount of injected $CO_2$ as well as the rate of the $CO_2$ injection was considered. It was observed that for the quantities of $CO_2$ used here, the amount of $CO_2$ injected has a large impact on the trapping. The residual trapping starts after the injection has ended, which gives the smaller amounts of injected $CO_2$ more time to redistribute and become trapped compared to when larger amounts of $CO_2$ is injected. Concerning the rate of injection, higher injection rate produced consistently more residual as well as overall trapping. When injecting a specified amount of $CO_2$, a higher injection rate corresponds to shorter injection duration and thereby a longer redistribution time in-situ and consequently more residual trapping.

Concerning alternative modes of injection the following could be observed: more $CO_2$ trapping occurs during the injection stage if co-injection of water is used. In addition, as can be expected, a larger mass percent of water does not only increase the residual and solubility trapping but also the pressure increase in-situ. When using chase water injection after $CO_2$ injection, the solubility trapping was increased by a few percent. The residual trapping was also enhanced greatly during the chase water injection, but with time the difference decreased being less than 10 percent at the end of the observation period.

When comparing various injection strategies against each other, but using similar $CO_2$/water injection rates a maximal difference of 0.12 in the TEI was seen 30 days after the start of the injection (Figure 6.30) Then, all strategies except cyclic injection had enhanced the trapping somewhat when compared with the conventional injection, mainly through increased residual trapping. Cyclic injection, as well as WAG injection strategies, can increase residual trapping greatly on a shorter time perspective. The highest pressure increase was seen for strategies which combined injection of both water and $CO_2$. When employing strategies consisting of chase water injections (strategy 2, 4 or 6), residually trapped $CO_2$ is lacking in the vicinity of the well due to dissolution into the liquid phase.

A comparison was also carried out how heterogeneity influences various modes of trapping: When sing the 2-D model it could be seen that short after the injection ends the trapping in the heterogeneous case (median TEI) is higher than for the homogeneous case. At the later times, however, the trapping becomes higher for the homogeneous case in comparison to most of the heterogeneous realizations. This is due to the fact that on longer time scales, heterogeneity is

retarding the buoyant migration which results in less imbibition and thereby less residually trapped CO2. The role of the two-dimensionality model in this result deserves further analysis.

A set of 3D simulations were also carried out, in order to evaluate the effect of certain selected injection strategies as well as geological heterogeneity on trapping. While being fully three-dimensional and thereby more representative of the true geology, the model also had some limitations in comparison to the previous 2D model, such as not including a hysteresis model. The model was therefore mainly at this stage used to look at dissolution trapping. Based on the 3D simulations following conclusions could be made: different injection patterns can be used to improve $CO_2$ dissolution trapping in saline aquifers. Injecting water after $CO_2$ injection, higher injection rate and having a pause in an injection cycle can be used to increase the $CO_2$ dissolution in the brine formation. It was also observed that dissolution index was higher in heterogeneous formations in comparison to homogeneous one.

The above simulations provide a good basis to decide which injection strategy to use at Heletz to achieve enhanced trapping. The final decision will be made once the first field results from the first set of simulations with 'conventional strategies' are available and can be used to calibrate the simulation models.

# 9. References


1. Aissaoui A., "Etude théorique et expérimentale de l'hydtérésis des pressions capillaires et des perméabilités relatives en vue du stockage souterrain de gaz", PhD of Ecole des Mines de Paris (1983), 223 p.
2. Benson, S.M., Pini, R., Krevor, S., Hingerl, F., Reynolds, C., Niu, B., Calvo, R., Niemi, A., Zuo, L., 2014. Relative permeability analyses to describe multi-phase flow in $CO_2$ storage reservoirs Part II: Resolving fundamental issues and filling data gaps. A research report prepared for the Global Carbon Capture and Storage Institute.
3. Bensabat, J., 2013. Characterization and monitoring of an injection experiment at Heletz Israel. Training Course on Geological Storage of $CO_2$ Gottingen, Germany $9^{th}$-$12^{th}$ October.
4. Doughty, C., 2008. User's guide for hysteretic capillary pressure and relative permeability functions in iTOUGH2. Earth Sciences Division. Lawrence Berkeley National Laboratory.
5. Erlström, M., Silva, O., de Vries, L.M., Shtivelman, V., Gendler, M., Goldberg, I.,Scadeanu, D., Sperber, C.M., 2010. Deliverable D022: 3D structures of test sites.MUSTANG, EU-FP7 proj. no. 227286, Public report avail. at www.co2mustang.eu
6. Fagerlund, F., Auli Niemi, Jacob Bensabat, Vladimir Shtivelman (2013) Interwell field test to determine in-situ CO2 trapping in a deep saline aquifer: Modelling study of the effects of test design and geological parameters. Energy Proc40, 554 – 563.
7. Fagerlund, F., Auli Niemi, Jacob Bensabat, Vladimir Shtivelman (2013) Design of a two-well field test to determine in situ residual and dissolution trapping of CO2 applied to the Heletz CO2 injection site. Int Jour Greenhouse Gas Control 19 (2013) 642–651
8. Finsterle, S., 2007. iTOUGH2 User's guide. LBNL-40040. Lawerence Berkeley National Laboratory, Berkeley.
9. Finsterle, S., Kowalsky, M.B., 2007. iTOUGH2-GSLIB User's Guide. LBNL-3191. Lawrence Berkeley National Laboratory, Berkeley.
10. van Genuchten, M. Th., 1980. A closed-form equation for predicting the hydraulic conductivity of unsaturated soil. Soil Society of America Journal, 44(5), 892-898.
11. Jerauld, G.R., 1997. Prudhoe Bay gas/oil relative permeability. SPE Reservoir Engineering 12(1), 66-73.
12. Land, C. S., 1968. Calculation of imbibition relative permeability for two- and three-phase flow from rock properties. SPE J, June 1968, 8(2): 149-156.
13. Lenhard, R.J., Parker, J.C., 1987. A model for hysteretic constitutive relations governing multiphase flow 2. permeability-saturation relations. Water Resources Research, 23(12), 2197-2206.
14. Niemi, A., Jacob Bensabat, Vladimir Shtivelman, Katriona Edlmann, Philippe Gouze, Linda Luquot, Ferdinand Hingerl, Sally M. Benson, Philippe A. Pezard, Kristina Rasmusson, Tian Liang, Fritjof Fagerlund, Michael Gendler, Igor Goldberg, Alexandru Tatomir, Torsten Lange, Martin Sauter and Barry Freifeld9 (2016) Heletz experimental site overview, characterization and data analysis for CO2 injection and geological storage. Submitted to International Journal of Greenhouse Gas Control (accepted with revision)
15. Nghiem, L., Yang, C., Shrivatava, V., Kohse, B., Hassam, M., Chen, D., Card, C., 2009. Optimization of residual gas and solubility trapping for $CO_2$ storage in saline aquifers. SPE 119080. Paper prepared for presentation at the 2009 SPE Reservoir Simulations Symposium held in Woodlands, Texas, USA, 2-4 February 2009.
16. Olofsson, C., 2011. The significance of heterogeneity for spreading of geologically stored carbon dioxide. Master thesis. Department of Earth Sciences, Uppsala University. ISSN 1401-5765.
17. Parker, J.C., Lenhard, R.J., 1987. A model for hysteretic constitutive relations governing multiphase flow 1. saturation-pressure relations. Water Resources Research, 23(12), 2187-2196.

18. Pruess, K., Oldenburg, C., Moridis, G., 1999. TOUGH2 User's guide, version 2.0, LBNL-43134. Lawrence Berkeley National Laboratory, Berkeley, CA.
19. Pruess K., 2005. ECO2N: A TOUGH2 fluid property module for mixtures of water, NaCl, and $CO_2$, LBNL-57952. Lawrence Berkeley National Laboratory, Berkeley, CA.
20. Rasmusson, K., Tsang, C.-F., Tsang, Y., Rasmusson M., Pan, L., Fagerlund, F., Bensabat, J., Niemi, A. (2015) Distribution of injected CO2 in a stratified saline reservoir accounting for coupled wellbore-reservoir flow. Greenhouse Gases: Science and Technology.Volume 5, Issue 4, August 2015, Pages: 419–436
21. Rasmusson, K,Rasmusson, M., Fagerlund, F., Bensabat,J., Tsang, Y. and Niemi, A. (2014) Analysis of alternative push-pull-test-designs for determining in-situ residual trapping of carbon dioxide. Int Jour Greenhouse Gas Control, Volume: 27 Pages: 155-168. Aug 2014
22. Spycher, N., Pruess, K., 2005. $CO_2$-$H_2O$ mixtures in the geological sequestration of $CO_2$. II. Partitioning in chloride brines at 12-100ºC and up to 600 bar. Geochimica et Cosmochimica Acta, 69(13), 3309-3320. doi: 10.1016/j.gca.2005.01.015.
23. Suzanne, K., Hamon, G., Billiote, J., Trocmé, V., 2003. Experimental relationships between residual gas saturation and initial gas saturation in heterogeneous sandstone reservoirs. SPE 84038. Paper prepared for presentation at the SPE Annual Technical Conference and Exhibition held in Denver, Colorado, USA, 5-8 October 2003.